



**NTNU – Trondheim**  
Norwegian University of  
Science and Technology

# Analysis of the Turbulent Energy Dissipation

**Olav Øyvind Førde**

Master of Science in Product Design and Manufacturing

Submission date: June 2012

Supervisor: Helge Ingolf Andersson, EPT

Norwegian University of Science and Technology  
Department of Energy and Process Engineering



EPT-M-2012-33

**MASTER THESIS**

for

student Olav Øyvind Førde

Spring 2012

Analysis of the turbulent energy dissipation

*Analyse av den turbulente energidissipasjonen***Background and objective**

The turbulent energy dissipation is an essential quantity in all turbulent flows. The energy dissipation prevents an unlimited growth of turbulence in a pipe or channel and makes grid-generated turbulence fade away. The turbulent energy dissipation is associated with the smallest turbulent eddies and are therefore not as readily accessible as the turbulent kinetic energy which primarily is associated with the large-scale motion. The objective of this thesis is to explore the turbulent energy dissipation by means of data from numerically simulated turbulent flow fields.

**The following tasks are to be considered:**

- 1 The candidate shall familiarize himself with the turbulent energy dissipation concept and how the dissipation rate is approximated in laboratory experiments and turbulence modeling where only limited information about the fluctuating three-dimensional flow field is available.
- 2 On the basis of data from three-dimensional computer simulations (Direct Numerical Simulations) deduce the different components of the energy dissipation tensor.
- 3 Examine the scalar dissipation in order to show how the 'correct' dissipation relates to the 'isotropic' dissipation as discussed by Bradshaw & Perot (Phys. Fluids 1993).
- 4 Deduce the energy dissipation rate from an under-resolved DNS and compare with data from a fully-resolved DNS.
- 5 Estimate the Kolmogorov length scale from the two simulations and compare with the mesh size. Decide if this comparison can be used to judge the adequacy of the grid resolution.
- 6 Introduce a length scale tensor analogous to the scalar Kolmogorov length scale. Discuss the implication of the directional dependence of the Kolmogorov length scale.

-- " --

Within 14 days of receiving the written text on the master thesis, the candidate shall submit a research plan for his project to the department.

When the thesis is evaluated, emphasis is put on processing of the results, and that they are presented in tabular and/or graphic form in a clear manner, and that they are analyzed carefully.

The thesis should be formulated as a research report with summary both in English and Norwegian, conclusion, literature references, table of contents etc. During the preparation of the text, the candidate should make an effort to produce a well-structured and easily readable report. In order to ease the evaluation of the thesis, it is important that the cross-references are correct. In the making of the report, strong emphasis should be placed on both a thorough discussion of the results and an orderly presentation.

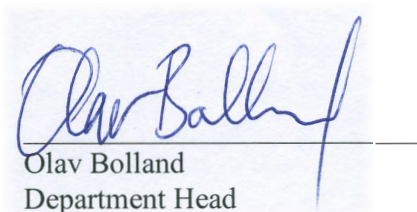
The candidate is requested to initiate and keep close contact with his/her academic supervisor(s) throughout the working period. The candidate must follow the rules and regulations of NTNU as well as passive directions given by the Department of Energy and Process Engineering.

Risk assessment of the candidate's work shall be carried out according to the department's procedures. The risk assessment must be documented and included as part of the final report. Events related to the candidate's work adversely affecting the health, safety or security, must be documented and included as part of the final report.

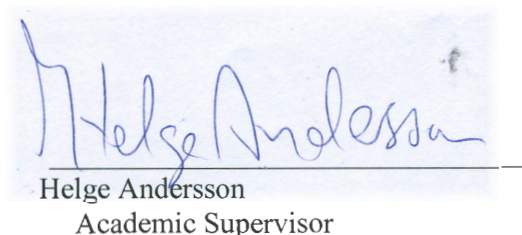
Pursuant to "Regulations concerning the supplementary provisions to the technology study program/Master of Science" at NTNU §20, the Department reserves the permission to utilize all the results and data for teaching and research purposes as well as in future publications.

The final report is to be submitted digitally in DAIM. An executive summary of the thesis including title, student's name, supervisor's name, year, department name, and NTNU's logo and name, shall be submitted to the department as a separate pdf file. Based on an agreement with the supervisor, the final report and other material and documents may be given to the supervisor in digital format.

Department of Energy and Process Engineering, 16. January 2012



Olav Bolland  
Department Head



Helge Andersson  
Academic Supervisor

Research Advisor:  
Dr. Mustafa Barri

## Abstract

An investigation of the turbulent fluctuating kinetic energy dissipation in low Reynolds number channel flow is made, both analytically and numerically with means of Direct Numerical Simulation (DNS). The unsteady Navier-Stokes equations are solved at a Reynolds number of 360, based on the shear velocity and channel height, for four grid resolutions  $48^3$ ,  $88^3$ ,  $128^3$  and  $192^3$ . The results are compared with data from Kim et al. (1987) [9], and good agreement is found for the  $192^3$  grid resolution.

The viscous term in the kinetic energy equation is derived and described, from there the “isotropic” dissipation equation is shown to be the homogeneous dissipation equation which is compared with the thermodynamically correct dissipation. The results are in agreement with the findings of Bradshaw and Perot (1993) [2], with a difference of maximum  $\approx 2.5\%$  from the correct dissipation.

The isotropic dissipation, often used as approximation in experiments, is also calculated and compared with the homogeneous dissipation. The results are unsurprisingly poor, and are only in agreement about the centerline. A comparison with an equation from the  $k$ - $\epsilon$ -model is also made, most as a curiosity, and also shows poor agreement.

The Kolmogorov length scale is calculated from the dissipation, and it shows clear grid dependency even though the grid is smaller than the Kolmogorov length scale in the  $z$ -direction with  $\max(\Delta z^+/\eta^+) = 0.8$ . The dissipation of the Reynolds stress components are used to create Kolmogorov length scales in  $x$ ,  $y$  and  $z$ -direction. They are also grid dependent, even though  $\max(\Delta z^+/\eta_{33}^+) \approx 0.7$ .

A length scale tensor analogous to the Kolmogorov length scale is proposed. It is based on the connection between the Reynolds stress equation and the turbulent fluctuating kinetic energy equation. It relaxes the grid restrictions compared to the Kolmogorov length scale, but investigation of its validity requires simulations with a super computer and is therefore not performed.

## Sammendrag

Det er gjennomført en undersøkelse av den turbulente fluktuerende kinetiske energidissipasjonen, både analytisk og numerisk med Direkte Numerisk Simulering (DNS). De tidsavhengige “Navier-Stokes”-ligningene er løst ved Reynolds tall lik 360, basert på skjærhastighet og kanalhøyde, for gridoppløsning på  $48^3$ ,  $88^3$ ,  $128^3$  og  $192^3$ . Resultatene er sammenlignet med data fra Kim et al. [9], og god overensstemmelse er funnet for  $192^3$  oppløsningen.

Det viskøse leddet i “kinetisk energi”-ligningen er utledet og forklart, og derfra er ligningen for “isotropisk” dissipasjon vist å være lik den homogene dissipasjonen, som sammenlignes med den termodynamisk korrekte dissipasjonen. Resultatene er i overensstemmelse med funnene til Bradshaw og Perot (1993) [2], med en differanse på maksimum  $\approx 2.5\%$  av den korrekte dissipasjonen.

Den isotropiske dissipasjonen, som ofte brukes ved eksperimenter, er også beregnet og sammenlignet med den homogene dissipasjonen. Resultatene er, ikke overraskende, dårlige og stemmer kun overens rundt senterlinjen. En sammeligning med  $k$ - $\epsilon$ -modellen er også gjort, mest som en kuriositet, og viser dårlige resultater.

Kolmogorovs lengdeskala er beregnet fra dissipasjonen og viser klar gridavhengighet, til tross for at gridet er mindre enn Kolmogorovs lengdeskala i  $z$ -retningen, med  $\max(\Delta z^+/\eta_{33}^+) \approx 0.8$ . Dissipasjonen av Reynoldsspenningens komponenter er brukt til å lage en Kolmogorov lengdeskala i  $x$ -,  $y$ - og  $z$ -retning. De er også gridavhengig til tross for at  $\max(\Delta z^+/\eta_{33}^+) \approx 0.7$ .

En tensor for lengdeskalaen er foreslått. Den er basert på forbindelsen mellom Reynoldsspenningen og den turbulente fluktuerende energiligningen. Den foreslåtte tensoren stiller mindre krav til gridoppløsning, men dens gyldighet er ikke undersøkt ettersom superdatamaskinen ikke var tilgjengelig.

## Preface

The work performed in this master thesis have been academically challenging and rewarding, and as a student of fluid dynamics it has been very exciting to work with DNS, an unusual task for a master thesis. The equations of fluid dynamics and turbulence are complex and intertwined, and getting a grasp of how they all are connected to one another was quite an obstacle. Another challenge was the lack of relevant research papers, as it appears no one else has studied the connection between the grid size and Kolmogorov length scale. Initially it was also believed that the super computer would be available for use, but it was unavailable this spring and therefore not all simulations which was planned could be made. I have spent many pages describing the equation of turbulent kinetic energy, because the viscous terms and their treatment lays the basis for the whole thesis and hopefully it is clear what I want to show.

I want to thank Prof. Helge I. Andersson for proposing this thesis and for good guidance. I also want to thank Post Doc. Mustafa Barri for all the help and time he has given me. Lastly I wish to thank Dr. Magnar Førde for helpful discussions and input.

June 11, 2012. Trondheim.  
Olav Øyvind Førde





# Contents

Background and Objective . . . . .	i
Abstract . . . . .	iii
Sammendrag . . . . .	iv
Preface . . . . .	v
List of Figures . . . . .	ix
Nomenclature . . . . .	x
<b>1 Theory</b>	<b>1</b>
1.1 Equations of Fluid Dynamics . . . . .	1
1.2 Equations of Turbulence . . . . .	2
1.3 Transfer of Kinetic Energy . . . . .	6
1.4 Measuring Dissipation in Experiments . . . . .	9
1.5 Dissipation in Turbulence Modelling . . . . .	14
<b>2 Direct Numerical Simulation</b>	<b>17</b>
2.1 Flow Domain and Equations . . . . .	17
2.2 Discretization Schemes . . . . .	18
2.3 Grid Resolution . . . . .	20
<b>3 Results - Turbulence Statistics</b>	<b>23</b>
3.1 Mean Flow Properties . . . . .	24
3.2 Turbulence Intensities . . . . .	26
3.3 Reynolds Shear Stress . . . . .	27
3.4 Turbulent Dissipation . . . . .	28
3.5 Kolmogorov Length Scale . . . . .	32
3.6 Turbulent Kinetic Energy Budget . . . . .	34
<b>4 Discussion</b>	<b>37</b>
4.1 Approximating Dissipation . . . . .	37
4.2 Dissipation . . . . .	38
4.3 Kolmogorov Length Scale . . . . .	39
4.4 Further Work . . . . .	41
4.5 Conclusion . . . . .	42
Bibliography . . . . .	44



# List of Figures

1.1	Energy transfer between scales . . . . .	7
1.2	Illustration of the breakdown of scales . . . . .	8
1.3	A probe used for hot-wire anemometry . . . . .	10
1.4	Ultrasonic velocimeter . . . . .	11
1.5	Illustrations of the PIV method . . . . .	12
2.1	Schematic of the flow domain . . . . .	17
2.2	Discretized domain in z-direction . . . . .	18
2.3	$\Delta z^+$ for different grid resolutions . . . . .	21
3.1	A time averaged and an instantaneous velocity field . . . . .	23
3.2	Mean velocity profile . . . . .	24
3.3	Near-wall mean velocity profile . . . . .	25
3.4	RMS of velocity components . . . . .	26
3.5	Shear forces . . . . .	27
3.6	Homogeneous dissipation . . . . .	28
3.7	Homogeneous vs. thermodynamical dissipation . . . . .	29
3.8	Homogeneous vs. isotropic dissipation . . . . .	30
3.9	Log-law region and dissipation . . . . .	31
3.10	Kolmogorov length scale . . . . .	32
3.11	The ratio of cell size to the Kolmogorov length scale . . . . .	33
3.12	$\Delta/\eta^+$ for different grid resolutions . . . . .	34
3.13	The turbulent kinetic energy budget . . . . .	35

## Nomenclature

$\rho$	density ( $\text{kg}/\text{m}^3$ )
$i$	subscript: axis direction, velocity component
+	superscript: wall scaled variable
$\alpha$	scaling parameter
$t$	time (s)
$\vec{u}$	velocity vector (m/s)
$u$	velocity in x-direction (m/s)
$v$	velocity in y-direction (m/s)
$w$	velocity in z-direction (m/s)
$\tilde{\phi}$	instantaneous variable
$\Phi$	upper case, time averaged variable
$\phi$	lower case, fluctuating variable
$\overline{\phi}$	time averaging
$p$	pressure ( $\text{N}/\text{m}^2$ )
$\mu$	molecular viscosity ( $\text{kg}/(\text{m}\cdot\text{s})$ )
$\mu_t$	“molecular” turbulent/eddy viscosity ( $\text{kg}/(\text{m}\cdot\text{s})$ )
$\nu$	kinematic viscosity ( $\text{m}^2/\text{s}$ )
$\nu_t$	turbulent/eddy viscosity ( $\text{m}^2/\text{s}$ )
$\vec{f}$	body force vector ( $\text{N m}^3/\text{kg}$ )
$k$	turbulence kinetic energy ( $\text{m}^2/\text{s}^2$ )
$\epsilon$	dissipation rate ( $\text{m}^2/\text{s}^3$ )
$L$	characteristic length (m)
$\kappa$	von Kármán constant
$\eta$	Kolmogorov length scale (m)
$\delta_{ij}$	Kronecker delta function
$\tau_{ij}^t$	Reynolds stress tensor ( $\text{m}^2/\text{s}^2$ )

# Chapter 1

## Theory

### 1.1 Equations of Fluid Dynamics

All governing equations used in fluid dynamics originates from the pillars of classical mechanics, the conservations laws. The conservation laws can be divided into conservation of mass, conservation of linear momentum and conservation of energy, where the two latter are of course Newton's Second Law of Motion and the First Law of Thermodynamics. These conservation laws are applied to an infinitesimally small control volume. This control volume is small enough to encapsulate what we call a fluid element, but not so small that intermolecular actions are of importance, i.e the Knudsen number has to be small.<sup>1</sup> From these conservation laws and the control volume we get the continuity equation, momentum equations and the energy equation. See chapter 2 in [1] and [22] for details.

$$\frac{\partial \rho}{\partial t} + \frac{\partial \rho u_i}{\partial x_i} = 0 \quad (1.1)$$

$$\frac{\partial \rho u_i}{\partial t} + \frac{\partial \rho u_i u_j}{\partial x_j} = -\frac{\partial p}{\partial x_i} + \frac{\partial \tau_{ji}}{\partial x_j} + \rho f_i \quad (1.2)$$

$$\frac{\partial \rho e}{\partial t} + \frac{\partial \rho e u_i}{\partial x_i} = k \frac{\partial^2 T}{\partial x_i^2} - \frac{\partial p u_i}{\partial x_i} + \frac{\partial \tau_{ji} u_i}{\partial x_i} + \rho f_i u_i + \rho \dot{q} \quad (1.3)$$

These are the general equations of fluid dynamics, but in this thesis we deal with an incompressible Newtonian fluid. This implies zero volumetric deformation and that the viscous stresses are proportional to the rate of deformation.

$$\frac{\partial u_i}{\partial x_i} = 0 \quad (1.4)$$

---

<sup>1</sup> $Kn = \frac{\lambda}{L}$  The ratio of the molecular mean free path and a representative physical length scale

$$\tau_{ji} = \tau_{ij} = \mu \left( \frac{\partial u_i}{\partial x_j} + \frac{\partial u_j}{\partial x_i} \right) \quad (1.5)$$

Hence the final equations becomes

$$\frac{\partial u_i}{\partial x_i} = 0 \quad (1.6)$$

$$\rho \left( \frac{\partial u_i}{\partial t} + u_j \frac{\partial u_i}{\partial x_j} \right) = -\frac{\partial p}{\partial x_i} + 2\mu \frac{\partial}{\partial x_j} s_{ij} \quad (1.7)$$

where  $s_{ij} = \frac{1}{2} \left( \frac{\partial u_i}{\partial x_j} + \frac{\partial u_j}{\partial x_i} \right)$  is the strain-rate tensor. Since we do not solve the energy/temperature equation we omit the details of that equation here, as well as gravity or body forces in the momentum equation.

## 1.2 Equations of Turbulence

### 1.2.1 Fluctuating turbulent kinetic energy

To investigate the dissipation of turbulent energy we need an equation to represent the turbulent kinetic energy. This is usually achieved by the so-called Reynolds decomposition, where the instantaneous flow is described by a time-averaged variable and a fluctuating variable.

$$\tilde{\phi} = \Phi + \phi \quad (1.8)$$

where  $\Phi$  by definition is:

$$\Phi \equiv \frac{1}{T} \int_{t_0}^{t_0+T} \tilde{\phi} dt \quad (1.9)$$

We can now derive from the instantaneous momentum equation 1.11 a decomposed equation.

$$\rho \left( \frac{\partial}{\partial t} (U_i + u_i) + (U_j + u_j) \frac{\partial}{\partial x_j} (U_i + u_i) \right) = -\frac{\partial}{\partial x_i} (P + p) + 2\mu \frac{\partial}{\partial x_j} (S_{ij} + s_{ij}) \quad (1.10)$$

We expand the equation:

$$\frac{\partial U_i}{\partial t} + \frac{\partial u_i}{\partial t} + U_j \frac{\partial U_i}{\partial x_j} + U_j \frac{\partial u_i}{\partial x_j} + u_j \frac{\partial U_i}{\partial x_j} + u_j \frac{\partial u_i}{\partial x_j} = -\frac{1}{\rho} \frac{\partial}{\partial x_i} (P + p) + 2\nu \frac{\partial}{\partial x_j} (S_{ij} + s_{ij}) \quad (1.11)$$

Multiplying the whole equation by  $u_i$  and time average will result in a Reynolds Averaged equation:

$$\begin{aligned} \overline{u_i \frac{\partial U_i}{\partial t}} + \overline{u_i \frac{\partial u_i}{\partial t}} + \overline{u_i U_j \frac{\partial U_i}{\partial x_j}} + \overline{u_i U_j \frac{\partial u_i}{\partial x_j}} + \overline{u_i u_j \frac{\partial U_i}{\partial x_j}} + \overline{u_i u_j \frac{\partial u_i}{\partial x_j}} \\ = -\frac{u_i}{\rho} \frac{\partial}{\partial x_i} (P + p) + 2\nu u_i \frac{\partial}{\partial x_j} (S_{ij} + s_{ij}) \end{aligned} \quad (1.12)$$

Utilizing  $\bar{U} = U$ ,  $\bar{u} = 0$ ,  $\overline{Uu} = \bar{U}\bar{u} = 0$  and  $\overline{uu} \neq 0$  we can simplify equation 1.12.

$$\begin{aligned} \overline{u_i \frac{\partial U_i}{\partial t}} &= \bar{u}_i \frac{\partial \bar{U}_i}{\partial t} = 0 \cdot \frac{\partial U_i}{\partial t} = 0 \\ \overline{u_i \frac{\partial u_i}{\partial t}} &= \overline{\frac{\partial}{\partial t} \frac{1}{2} u_i u_i} = \frac{\partial k}{\partial t}, \text{ where } k = \frac{1}{2} \overline{u_i u_i} \\ \overline{u_i U_j \frac{\partial U_i}{\partial x_j}} &= 0 \\ \overline{u_i U_j \frac{\partial u_i}{\partial x_j}} &= U_j \frac{\partial k}{\partial x_j} \\ \overline{u_i u_j \frac{\partial U_i}{\partial x_j}} &= \overline{u_i u_j} \frac{1}{2} \left( \frac{\partial U_i}{\partial x_j} + \frac{\partial U_j}{\partial x_i} \right) = \overline{u_i u_j} S_{ij} \\ \overline{u_i u_j \frac{\partial u_i}{\partial x_j}} &= \frac{\partial}{\partial x_j} \left( \frac{1}{2} \overline{u_i u_i u_j} \right) \\ -\frac{u_i}{\rho} \frac{\partial}{\partial x_i} (P + p) &= -\frac{\partial}{\partial x_i} (\overline{u_i p}) \\ \overline{2\nu u_i \frac{\partial}{\partial x_j} (S_{ij} + s_{ij})} &= 2\nu \frac{\partial}{\partial x_j} (\overline{u_j s_{ij}}) - 2\nu \overline{s_{ij} s_{ij}} \end{aligned} \quad (1.13)$$

Inserting these results into equation 1.12 gives the kinetic energy equation for turbulence fluctuations.

$$\frac{\partial k}{\partial t} + U_j \frac{\partial k}{\partial x_j} = -\frac{\partial}{\partial x_j} \left[ \frac{1}{\rho} \overline{u_j p} + \frac{1}{2} \overline{u_i u_i u_j} - 2\nu \overline{u_i s_{ij}} \right] - \overline{u_i u_j} S_{ij} - 2\nu \overline{s_{ij} s_{ij}} \quad (1.14)$$

### 1.2.2 Viscous terms and dissipation

This is however an inconvenient form of the equation for a study of the viscous term, as it is split up in two terms. We insert instead the term almost as it

appears on the left side in equation 1.13, except for a simple change:

$$\overline{2\nu u_i \frac{\partial}{\partial x_j} (S_{ij} + s_{ij})} = \overline{2\nu u_i \frac{\partial}{\partial x_j} s_{ij}} = \overline{\nu u_i \frac{\partial^2 u_i}{\partial x_j^2}} \quad (1.15)$$

$$\frac{\partial k}{\partial t} + U_j \frac{\partial k}{\partial x_j} = - \frac{\partial}{\partial x_j} \left[ \frac{1}{\rho} \overline{u_j p} + \frac{1}{2} \overline{u_i u_i u_j} \right] - \overline{u_i u_j S_{ij}} + \overline{\nu u_i \frac{\partial^2 u_i}{\partial x_j^2}} \quad (1.16)$$

Since equation 1.16 is a transport equation the viscous term consists of two different effects, a sink/source effect and a transport effect. [4] It behaves as a sink as it describes the rate of dissipation of turbulent energy to heat as well as it describes the rate of transport of turbulent energy by viscous forces, hence:

$$\overline{\nu u_i \frac{\partial^2 u_i}{\partial x_j^2}} = T - \phi \quad (1.17)$$

Where  $\phi$  is the fluctuations of the decomposed and time averaged general dissipation function:

$$\epsilon = \Phi + \phi = \nu \overline{\frac{\partial U_i}{\partial x_j} \left( \frac{\partial U_i}{\partial x_j} + \frac{\partial U_j}{\partial x_i} \right)} + \nu \overline{\frac{\partial u_i}{\partial x_j} \left( \frac{\partial u_i}{\partial x_j} + \frac{\partial u_j}{\partial x_i} \right)} \quad (1.18)$$

We insert  $\phi$  back into 1.17

$$\overline{\nu u_i \frac{\partial^2 u_i}{\partial x_j^2}} = T - \nu \overline{\frac{\partial u_i}{\partial x_j} \left( \frac{\partial u_i}{\partial x_j} + \frac{\partial u_j}{\partial x_i} \right)} \quad (1.19)$$

And take a closer look at how we can rearrange the left hand side:

$$\nu \overline{\frac{\partial^2 \frac{1}{2} u_i^2}{\partial x_j^2}} = \nu \frac{\partial}{\partial x_j} \overline{\left( u_i \frac{\partial u_i}{\partial x_j} \right)} = \nu \overline{\frac{\partial u_i}{\partial x_j} \frac{\partial u_i}{\partial x_j}} + \overline{\nu u_i \frac{\partial^2 u_i}{\partial x_j^2}} \quad (1.20)$$

$$\overline{\nu u_i \frac{\partial^2 u_i}{\partial x_j^2}} = \underbrace{\nu \overline{\frac{\partial^2 \frac{1}{2} u_i^2}{\partial x_j^2}}}_{\text{Incomplete transport}} - \underbrace{\nu \overline{\frac{\partial u_i}{\partial x_j} \frac{\partial u_i}{\partial x_j}}}_{\text{Homogeneous dissipation}} \quad (1.21)$$

Now we have two different equations for the viscous term, equations 1.19 and 1.21, and can therefore solve for T.

$$\nu \overline{\frac{\partial^2 \frac{1}{2} u_i^2}{\partial x_j^2}} - \nu \overline{\frac{\partial u_i}{\partial x_j} \frac{\partial u_i}{\partial x_j}} = T - \nu \overline{\frac{\partial u_i}{\partial x_j} \left( \frac{\partial u_i}{\partial x_j} + \frac{\partial u_j}{\partial x_i} \right)} \quad (1.22)$$

$$T = \nu \overline{\frac{\partial^2 \frac{1}{2} u_i^2}{\partial x_j^2}} + \nu \overline{\frac{\partial^2 u_i u_j}{\partial x_i \partial x_j}} \quad (1.23)$$



Finally we end up with the following expression for the viscous term:

$$\overline{\nu u_i \frac{\partial^2 u_i}{\partial x_j^2}} = \underbrace{\nu \left( \frac{\partial^2 k}{\partial x_j^2} + \frac{\partial^2 u_i u_j}{\partial x_i \partial x_j} \right)}_{\text{Full transport}} - \underbrace{\nu \frac{\partial u_i}{\partial x_j} \left( \frac{\partial u_i}{\partial x_j} + \frac{\partial u_j}{\partial x_i} \right)}_{\text{Correct dissipation}} \quad (1.24)$$

This equation describes the correct physical behavior of the viscous term in the equation for fluctuating turbulent kinetic energy, with the point being that the commonly used equation 1.21 is incorrect when discussing inhomogeneous dissipation. [4] The dissipation in equation 1.21 is often called the “isotropic dissipation”, which also is inaccurate, as the only condition needed to achieve this mathematical form from the correct dissipation term is homogeneity. [2] Isotropic turbulence implies that the statistical correlations are independent of direction, e.g. the velocity fluctuations are equal along the x-, y- and z-axis independent of the coordinate system’s position and angle. Homogeneous turbulence implies that the spatial derivatives of all mean turbulence quantities are zero, i.e. the quantities are independent of spatial position. To see that the condition of homogeneity suffices we can look at the kinetic energy equation again with the condition applied. Equation 1.14 reduces to:

$$\frac{\partial k}{\partial t} = -\overline{u_i u_j} S_{ij} - 2\nu \overline{s_{ij} s_{ij}} \quad (1.25)$$

and equation 1.16

$$\frac{\partial k}{\partial t} = -\overline{u_i u_j} S_{ij} + \nu u_i \overline{\frac{\partial^2 u_i}{\partial x_j^2}} \quad (1.26)$$

But with homogeneous turbulence the last term in equation 1.26 reduces to:

$$\nu u_i \overline{\frac{\partial^2 u_i}{\partial x_j^2}} = -\nu \overline{\frac{\partial u_i}{\partial x_j} \frac{\partial u_i}{\partial x_j}} \quad (1.27)$$

which can be seen from equation 1.21. And we see that for homogeneous turbulence we get the simplification

$$\epsilon = 2\nu \overline{s_{ij} s_{ij}} = \nu \overline{\frac{\partial u_i}{\partial x_j} \left( \frac{\partial u_i}{\partial x_j} + \frac{\partial u_j}{\partial x_i} \right)} = \nu \overline{\frac{\partial u_i}{\partial x_j} \frac{\partial u_i}{\partial x_j}} \quad (1.28)$$

This simplification is often utilized in turbulence models, as its transport equation is much less complicated than for the full term. This homogeneous dissipation term will also be subject to investigation later in the thesis, where a comparison with the thermodynamically correct dissipation will be made.

### 1.2.3 Reynolds Stresses

The derivation of the Reynolds stresses is long, tedious and very similar to the derivation of equation 1.14 and therefore omitted, but see [5] for details. The steady transport equations for the Reynolds stresses are

$$\begin{aligned} \frac{\partial}{\partial x_k} (\bar{U}_k \bar{u}_i \bar{u}_j) &= -\bar{u}_i \bar{u}_k \frac{\partial \bar{U}_i}{\partial x_k} - \bar{u}_i \bar{u}_k \frac{\partial \bar{U}_j}{\partial x_k} \\ -\frac{\partial}{\partial x_k} &\left( \bar{u}_i \bar{u}_j \bar{u}_k + \frac{1}{\rho} \delta_{jk} \bar{u}_i \bar{p} + \frac{1}{\rho} \delta_{ik} \bar{u}_j \bar{p} - \nu \frac{\partial \bar{u}_i \bar{u}_j}{\partial x_k} \right) \\ &+ \frac{1}{\rho} \overline{p \left( \frac{\partial u_i}{\partial x_j} + \frac{\partial u_j}{\partial x_i} \right)} - \underbrace{2\nu \overline{\frac{\partial u_i}{\partial x_k} \frac{\partial u_j}{\partial x_k}}}_{\text{Dissipation}} \end{aligned} \quad (1.29)$$

Solving these equations yields the symmetric Reynolds stress tensor,  $\tau_{ij} = \bar{u}_i \bar{u}_j$ . By taking the trace of this tensor and dividing by two, we get the equation for the fluctuating kinetic energy, i.e  $k = \frac{1}{2} \bar{u}_i \bar{u}_j \delta_{ij}$ , where  $\delta_{ij}$  is the Kronecker delta. We also observe that the dissipation term is not equal the correct dissipation, consider again the trace of the Reynolds stress tensor, the dissipation term will then be

$$2\nu \overline{\frac{\partial u_i}{\partial x_k} \frac{\partial u_j}{\partial x_k}} \delta_{ij} = 2\nu \overline{\frac{\partial u_i}{\partial x_k} \frac{\partial u_i}{\partial x_k}} \quad (1.30)$$

The trace of the dissipation term in the Reynolds stress tensor is twice the homogeneous dissipation, and hence

$$\epsilon = 0.5(\epsilon_{11} + \epsilon_{22} + \epsilon_{33}) \quad (1.31)$$

So the norm of calculating the dissipation in DNS from the Reynolds stresses is inaccurate, but this inaccuracy will be quantified later.

## 1.3 Transfer of Kinetic Energy

Turbulence is an energy demanding property of the flow due to several reasons, e.g. an increase in (wall) shear stress and deformation work. The turbulent kinetic energy distribution can be divided into production, diffusion and dissipation, i.e. energy absorbed, redistributed and energy lost through heat due to viscous forces. The kinetic energy is produced in and transferred from the mean flow to the fluctuating flow and lost by a heat increase through what is called the energy cascade. This energy transfer is described by the interaction of motion of different scales, and these motions are usually called eddies. An eddy is a loose

term collecting identifiable turbulent patterns such as velocity and pressure into one term. We can observe the kinetic energy transfer by identifying terms in the equations of mean and fluctuating kinetic energy.

$$\frac{\partial k}{\partial t} + U_j \frac{\partial k}{\partial x_j} = - \frac{\partial}{\partial x_j} \left[ \frac{1}{\rho} \overline{u_j p} + \frac{1}{2} \overline{u_i u_i u_j} - 2\nu \overline{u_i s_{ij}} \right] - \underbrace{\overline{u_i u_j} S_{ij}}_{\text{source}} - 2\nu \overline{s_{ij} s_{ij}} \quad (1.32)$$

$$\frac{\partial K}{\partial t} + U_j \frac{\partial K}{\partial x_j} = - \frac{\partial}{\partial x_j} \left[ \frac{1}{\rho} \overline{U_j p} + \frac{1}{2} \overline{U_i u_i u_j} - 2\nu \overline{U_i S_{ij}} \right] + \underbrace{\overline{u_i u_j} S_{ij}}_{\text{sink}} - 2\nu \overline{S_{ij} S_{ij}} \quad (1.33)$$

Here we notice that the same term appear in both equations, only with opposite sign. This in addition with the fact that  $\overline{u_i u_j} S_{ij}$  is almost always negative, this relation shows that energy is transferred from the mean flow to the fluctuations. Why this term is mostly negative can be explained by using kinetic theory of gases. Figure 1.1 shows the transfer of energy between the different equations,

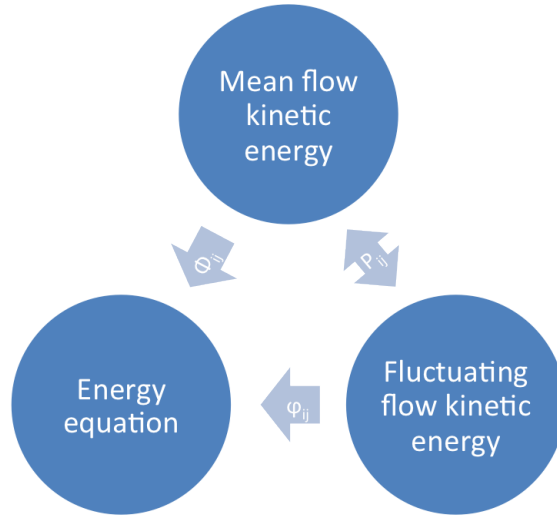


**Figure 1.1:** The transfer of energy between different scales and components of the flow

i.e. the mean flow, the fluctuating flow and the energy equation. The energy which goes into the energy equation, i.e. the dissipation, represents an irreversible loss through heat. To further increase our understanding of how a turbulent flow behaves, we can look at the concept of turbulent scales introduced by Kolmogorov in 1941 [10], which builds on the ideas of Richardson. [17]

### 1.3.1 Turbulence Scales and the Energy Cascade

The basic idea of Richardson was that the smaller turbulent structures feed of the energy from the larger energy containing turbulent structures, and he probably explains it best with his famous poem:

Big whirls have little whirls,  
 Which feed on their velocity,  
 And little whirls have lesser whirls,  
 And so on to viscosity.  
 - *L.F Richardson*

Figure 1.2 illustrates the energy cascade, a breakup of unstable large eddies or whirls which continues until the forces of viscosity stabilizes the eddies and energy leave the flow through molecular viscosity causing an entropy increase. Kolmogorov was among the first to quantify this energy transfer down the energy cascade with the assumption of homogeneous, isotropic turbulence and high Reynolds number.

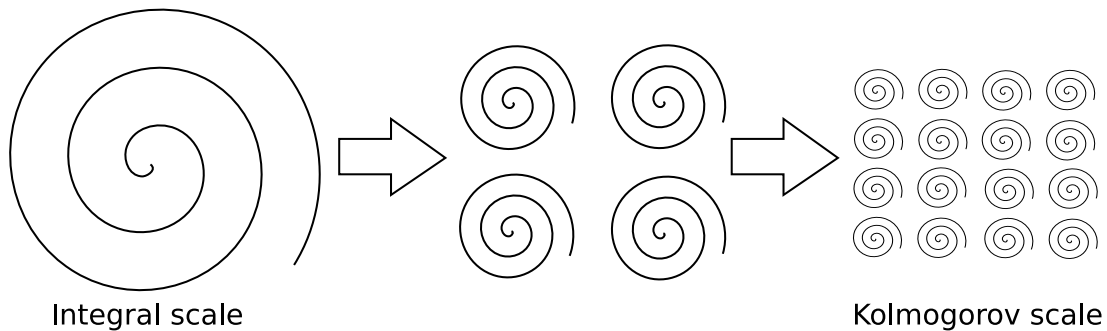


**Figure 1.2:** Illustration of the breakdown of scales

### Integral Scales

The integral scales of length, time and velocity are denoted by  $l$ ,  $t = l/u$  and  $u$ . These are the characteristics of the flow determined by the imposed geometry. For example in a pipe the length scale of the largest eddy would equal the diameter. The integral scales can thus be seen as the boundary conditions of the flow, and they are specific to the flow situation in question. The Reynolds number with the integral scales is  $Re = \frac{UL}{\nu}$ .

### Kolmogorov Scales

The Kolmogorov micro scales are the scales at which the smallest turbulent motion exist before they are dissipated by viscous effects. Observing that these small-scale motions have very small time scales, it can be assumed that these motions are statistically independent of the large-scale turbulence which has a long turn-over time. From here Kolmogorov stated that the small scales should only be dependent on the energy supplied from the large scales and the viscosity, but the supplied energy must equal the dissipated energy and therefore the small scales are a function of dissipation and viscosity. Utilizing this fact together with

dimensional analysis these expressions can be inferred for the scales of length,  $\eta$ , time,  $\tau$ , and velocity,  $v$ :

$$\eta = \left(\frac{\nu^3}{\epsilon}\right)^{1/4} \quad \tau = \left(\frac{\nu}{\epsilon}\right)^{1/2} \quad v = (\nu\epsilon)^{1/4} \quad (1.34)$$

If we insert these variables into the expression for the Reynolds number we get:

$$\text{Re} = \frac{1}{\nu}(\nu\epsilon)^{1/4} \left(\frac{\nu^3}{\epsilon}\right)^{1/4} = \frac{1}{\nu} \left(\frac{\nu\epsilon\nu^3}{\epsilon}\right)^{1/4} = 1 \quad (1.35)$$

This Reynolds number shows that the viscous effects are always important at these scales. It is also interesting to see the ratio of the small-scale to the large-scale, but in order to do that we need another way of describing  $\eta$ , i.e. an expression for the dissipation  $\epsilon$  is needed. Following the arguments of Tennekes and Lumley [21] we start with the assumption that the rate of the energy supplied<sup>2</sup> to small eddies is proportional to the reciprocal of the time scale of the integral scale. The integral time scale is  $l/u$ , and the kinetic energy per unit mass in the integral scale is  $u^2$ . Thus will the rate of energy supply from the large scale be proportional to  $u^3/l$  and:

$$\epsilon \sim \frac{U^3}{L} \quad (1.36)$$

Now we are equipped to compare the integral and Kolmogorov scales:

$$\frac{\eta}{l} = \text{Re}^{-3/4} \quad \frac{\tau}{t} = \text{Re}^{-1/2} \quad \frac{v}{u} = \text{Re}^{-1/4} \quad (1.37)$$

We see that the difference between the scales increases with the Reynolds number, and could appear to reach the limit zero. But it is important to remember that turbulence is a continuum phenomenon as long as we avoid simultaneously a high Mach number and low Reynolds number, a situation unlikely to occur on earth.

## 1.4 Measuring Dissipation in Experiments

To measure dissipation by experiments is one of the most difficult tasks in fluid dynamics today. The fidelity demanded by the experiments to yield accurate values of the velocity fluctuations is the most demanding part, mainly because of the three-dimensional behavior of turbulence as well as the small scales at which dissipation occurs. Today there are three main methods to measure velocity of a flow; hot-wire anemometer, supersonic anemometer and particle image velocimetry (PIV).

---

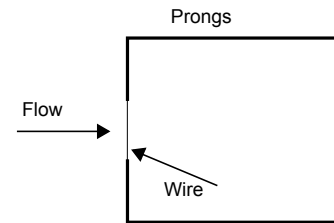
<sup>2</sup>Rate of energy is energy per time unit

### 1.4.1 Hot-Wire Anemometry

This is an intrusive point-measurement method which utilizes knowledge about forced convection<sup>3</sup> and its relation to the surrounding fluid velocity. A wire is placed between two prongs and is subject to either a constant current or constant temperature. If the current is kept constant, then a change in flow velocity will cause variations in resistance which again is measured by monitoring voltage variations across the wire. If the temperature is kept constant then the change in current would be the variable to describe the flow velocity.

The advantages of hot-wire anemometry [3]:

- Low noise levels
- Quick, i.e. very good frequency response
- Allows temperature measurements
- Can be used for two phase flows



The disadvantages of hot-wire anemometry:

- Intrusive, i.e. it locally disturbs the flow field
- Insensitive to reversal of flow direction, e.g. for turbulent flows
- Wire extremely sensitive to deposition of impurities
- Weak structural strength of probe
- Point measurement, very demanding to map a complete flow field

**Figure 1.3:** A probe used for hot-wire anemometry

The probe can also be equipped with two or three wires, which would give information about direction of velocity as well. In the case of turbulent flow the fluctuating voltage is used to find the fluctuating velocity in the Reynolds decomposition. The wire length is the parameter that decide which scale you are measuring.

### 1.4.2 Ultrasonic Velocimeter

Ultrasonic anemometers are similar to the hot-wire anemometer, they also utilize the fact that change in fluid velocity change how information travels between two measuring points, e.g. the wire end points. Figure 1.4 shows the setup of the

<sup>3</sup>Conduction and radiation usually neglected

ultrasonic velocimeter. An ultrasonic sound pulse is sent from point 1 to point 2 and another pulse is sent back again to point 1 from point 2. The time those two pulses used to travel between the points are measured and the difference gives information about the velocity in the 1-2 direction. The same process repeats itself in the 3-4 direction, a pulse is sent out from point 3 to point 4 and a pulse is sent back from point 4 to point 3. This time difference then gives information about the velocity in the 3-4 direction.

In the case of figure 1.4 the pulse will travel faster from point 1 to point 2, than it will the opposite direction. It will also travel faster from point 3 to point 4, than it will from point 4 to point 3. Three-dimensional probes can also be applied. Some of the advantages of ultrasonic velocimetry are:

- Quick, i.e. very good frequency response
- Allows temperature measurements [11]

Some of the disadvantages are:

- Intrusive, i.e. it locally disturbs the flow field
- Point measurement, very demanding to map a complete flow field
- Low spatial resolution

### 1.4.3 Particle Image Velocimetry

PIV exploits the digitalization of cameras to map the velocity in planes and even volumes. Lasers are used to create an illuminated plane in a section of the flow, and the flow is filled with spherical particles which reflect the laser light. A high speed camera is used to take pictures of the illuminated particles moving in the plane allowing calculation of velocity of the particle displacement between two succeeding pictures. This calculation gives an instantaneous vector plot of the flow field.

Advantages of PIV:

- Non-intrusive, i.e. it does not affect the flow field
- Maps large regions of the flow

Disadvantages of PIV:

- High speed flows demands very expensive high speed cameras

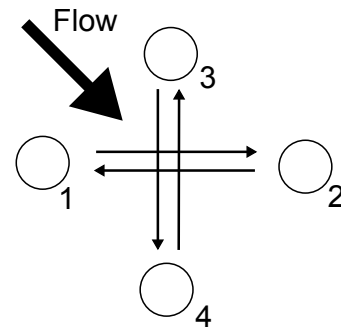
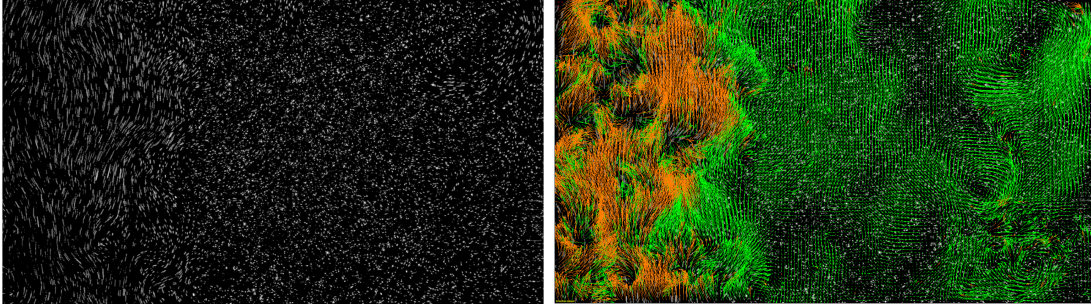


Figure 1.4



(a) Black and white photo of particles in a flow (b) Vector plot calculated from two succeeding pictures

**Figure 1.5:** Illustrations of the PIV method

- Lasers are also very expensive
- Can not measure through non-transparent walls
- Low spatial resolution

#### 1.4.4 Approximating Dissipation

As the three subsections above show it is very hard to measure the dissipation in flows because of the limited amount of data. How should the turbulent energy dissipation be approximated if velocity information is only available in certain points in space? Taylor [19] investigated in 1935 the simplifications arising in the general dissipation equation by assuming isotropic turbulence.

$$\begin{aligned} \nu \overline{\frac{\partial u_i}{\partial x_j} \left( \frac{\partial u_i}{\partial x_j} + \frac{\partial u_j}{\partial x_i} \right)} &= \nu \left( 2 \overline{\left( \frac{\partial u}{\partial x} \right)^2} + 2 \overline{\left( \frac{\partial v}{\partial y} \right)^2} + 2 \overline{\left( \frac{\partial w}{\partial z} \right)^2} + \overline{\left( \frac{\partial v}{\partial x} + \frac{\partial u}{\partial y} \right)^2} \right. \\ &\quad \left. + \overline{\left( \frac{\partial w}{\partial y} + \frac{\partial v}{\partial z} \right)^2} + \overline{\left( \frac{\partial u}{\partial z} + \frac{\partial w}{\partial x} \right)^2} \right) \end{aligned} \quad (1.38)$$

Remembering that isotropic turbulence implies that the average value of any function of the velocity is unchanged no matter how the axes are rotated, we get

$$\overline{\left( \frac{\partial u}{\partial x} \right)^2} = \overline{\left( \frac{\partial v}{\partial y} \right)^2} = \overline{\left( \frac{\partial w}{\partial z} \right)^2} \quad (1.39)$$

$$\overline{\left( \frac{\partial u}{\partial y} \right)^2} = \overline{\left( \frac{\partial u}{\partial z} \right)^2} = \overline{\left( \frac{\partial v}{\partial x} \right)^2} + \dots \quad (1.40)$$

$$\frac{\overline{\partial v \partial u}}{\partial x \partial y} = \frac{\overline{\partial w \partial v}}{\partial y \partial z} = \frac{\overline{\partial u \partial w}}{\partial z \partial x} \quad (1.41)$$



Adding these terms together results in

$$\epsilon = 6\nu \left( \overline{\left(\frac{\partial u}{\partial x}\right)^2} + \overline{\left(\frac{\partial u}{\partial y}\right)^2} + \overline{\frac{\partial v \partial u}{\partial x \partial y}} \right) \quad (1.42)$$

Taylor then used the continuity equation to show that

$$\overline{\left(\frac{\partial u}{\partial x}\right)^2} = -2 \overline{\frac{\partial v \partial u}{\partial x \partial y}} \quad (1.43)$$

Then through a long process of using linear algebra Taylor proves that the possible terms in equation 1.42 are linearly related to each other and that

$$2 \overline{\left(\frac{\partial u}{\partial x}\right)^2} = \overline{\left(\frac{\partial u}{\partial y}\right)^2} \quad (1.44)$$

Finally inserting these relations into equation 1.42 gives the dissipation equation for isotropic turbulence.

$$\epsilon = 15\nu \overline{\left(\frac{\partial u}{\partial x}\right)^2} \quad (1.45)$$

Now a simple and elegant equation for the dissipation is available, but unfortunately it consist of the *spatial* derivative of the velocity. However, when measuring velocity with a probe it is the *temporal* dependent velocity,  $u(t)$ , which is obtained. How can a spatial derivative be calculated from a “fixed in space”, time dependent variable? The answer is using Taylor’s frozen turbulence hypothesis [20], “*If the velocity of the air stream which carries the eddies is very much greater than the turbulent velocity, one may assume that the sequence of changes in  $u$  at the fixed point are simply due to the passage of an unchanging pattern of turbulent motion over the point.*” Thus we can write

$$u = u(t) = u(x/U) \quad (1.46)$$

Since the velocity fluctuations are frozen the substantive derivative equals zero

$$\begin{aligned} \overline{\frac{Du}{Dt}} &= \overline{\frac{\partial u}{\partial t}} + U \overline{\frac{\partial u}{\partial x}} = 0 \\ \overline{\frac{\partial u}{\partial x}} &= -\frac{1}{U} \overline{\frac{\partial u}{\partial t}} \end{aligned} \quad (1.47)$$

Note that the mean velocity  $U$  could be replaced with the instantaneous  $u'$  as proposed by Heskestad (1965) [8]. The negative sign makes physical sense, e.g. if the velocity of the flow coming from the left is increasing in time, then the

spatial derivative to the right have to be negative. Inserting this into equation 1.42 gives

$$\epsilon = 15\nu \overline{\left(\frac{1}{U} \frac{\partial u}{\partial t}\right)^2} \quad (1.48)$$

More advanced approximations exist, e.g. with assumptions of axi-symmetric or semi-isotropic turbulence, see [12] for details.

## 1.5 Dissipation in Turbulence Modelling

Closer investigation of equation 1.11, the Reynolds decomposed momentum equation, gives by time averaging:

$$\begin{aligned} \frac{\partial U_i}{\partial t} + \frac{\partial U_i U_j}{\partial x_j} + \frac{\overline{\partial u_i u_j}}{\partial x_j} &= -\frac{1}{\rho} \frac{\partial P}{\partial x_i} + 2\nu \frac{\partial}{\partial x_j} S_{ij} \\ \frac{\partial U_i}{\partial t} + \frac{\partial U_i U_j}{\partial x_j} &= -\frac{1}{\rho} \frac{\partial P}{\partial x_i} + \nu \frac{\partial^2 U_i}{\partial x_j^2} - \frac{\partial}{\partial x_j} \overline{u_i u_j} \end{aligned} \quad (1.49)$$

Still assuming an incompressible Newtonian fluid. This equation, known as the Reynolds Averaged Navier-Stokes equation, is the same as the original Navier-Stokes equation except for the symmetrical Reynolds stress  $\rho \overline{u_i u_j}$ .

$$\tau_{ij}^t \equiv -\rho \overline{u_i u_j} = -\rho \begin{pmatrix} \overline{u^2} & \overline{uv} & \overline{uw} \\ \overline{vu} & \overline{v^2} & \overline{vw} \\ \overline{wu} & \overline{wv} & \overline{w^2} \end{pmatrix} \quad (1.50)$$

It is the treatment of this term which is at the heart of the turbulence closure problem, there simply are no equations for the six new unknowns brought forward by the Reynolds stress. The Reynolds stress is dependent on the flow itself, and hence can not be described by constitutive relations as for example the viscous stress in a Newtonian flow, but turbulence modelling tries to exactly that in the best possible way. Over the years many methods have been developed, but the industry standard today is the two-equation  $k$ - $\epsilon$ -model based on the Boussinesq eddy viscosity hypothesis, see Pope [16] for a detailed discussion. The hypothesis states that the Reynolds stress anisotropy is equal the rate of strain tensor, which is analogous to the viscous stress relation:

$$-\overline{u_i u_j} = \nu_t \left( \frac{\partial U_i}{\partial x_j} + \frac{\partial U_j}{\partial x_i} \right) - \frac{2}{3} k \delta_{ij} \quad (1.51)$$

Where  $\nu_t$  is the eddy viscosity. Inserting this into equation 1.49 gives

$$\frac{\partial U_i}{\partial t} + \frac{\partial U_i U_j}{\partial x_j} = (\nu + \nu_t) \frac{\partial^2 U_i}{\partial x_j^2} - \frac{1}{\rho} \frac{\partial}{\partial x_i} \left( P + \frac{2}{3} \rho k \right) \quad (1.52)$$

This equation is solved using the  $k$ - $\epsilon$ -model, and in addition to the Boussinesq eddy viscosity hypothesis it employs a transport equation for  $k$ , a transport equation for  $\epsilon$  and from  $\nu_t = \nu_t(\text{length}, \text{velocity})$  it specifies  $\nu_t = C_\mu k^2 / \epsilon$ . The big limitation of this turbulence model, and in fact any model utilizing the Boussinesq eddy viscosity hypothesis, is that it is isotropic. Remembering that  $k = 0.5(u^2 + v^2 + w^2)$ , it is clear that all the velocity fluctuations are needed in order to calculate anisotropic turbulence, but with this model  $k$  is calculated directly, such that  $u^2 = v^2 = w^2$ . The transport equations of  $k$  and  $\epsilon$  are:

$$\frac{Dk}{Dt} = \nabla \cdot \left( \frac{\nu_t}{\sigma_k} \nabla k \right) + P - \epsilon \quad (1.53)$$

$$\frac{D\epsilon}{Dt} = \nabla \cdot \left( \frac{\nu_t}{\sigma_\epsilon} \nabla \epsilon \right) + C_1 \frac{P\epsilon}{k} - C_2 \frac{\epsilon^2}{k} \quad (1.54)$$

The transport equation for  $\epsilon$  is based on the same arguments as the energy cascade above, i.e. that the production and dissipation are proportional to the reciprocal of the large eddy turnover time,  $\epsilon/k$  [18]. Again looking to Pope [16] one can for the case of channel flow with homogeneous streamwise and spanwise turbulence derive the following relation:

$$\epsilon = \frac{C_\mu^{3/4} k^{3/2}}{\kappa y} \quad (1.55)$$

Where  $\kappa \approx 0.4$  is the von Kármán constant and  $C_\mu = 0.09$ . This relation is only valid within the log-law region where the production of turbulent kinetic energy is approximately equal to the dissipation.



# Chapter 2

## Direct Numerical Simulation

### 2.1 Flow Domain and Equations

The structure of the CFD-code used in this thesis has not been a subject of investigation, it is however presented here in the interest of the reader. Figure 2.1 illustrates the domain solved by means of Direct Numerical Simulation in this thesis, where  $L_x = 2\pi$ ,  $L_y = \pi$  and  $L_z = H = 1$  denotes the streamwise, spanwise and wall normal direction respectively. The Navier-Stokes equations are solved in their non-dimensional form, which means that the variables are scaled by their characteristic counter part. The star indicates a non-dimensional variable:

$$x^* = x/H \quad \vec{u}^* = \vec{u}/u_\tau \quad t^* = tu_\tau/L \quad p^* = p/(\rho u_\tau^2) \quad (2.1)$$

We insert these into equation 1.2:

$$\frac{\partial \rho u_i^* u_\tau}{\partial t^* H/u_\tau} + \frac{\partial \rho u_i^* u_\tau u_j^* u_\tau}{\partial x_j^* H} = -\frac{\partial p^* \rho u_\tau^2}{\partial x_i^* H} + \mu \frac{\partial^2 u_i^* u_\tau}{\partial x_j^* H \partial x_j^* H} \quad (2.2)$$

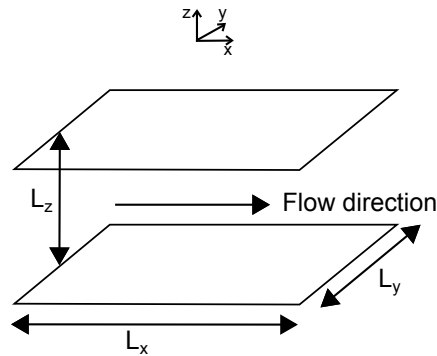
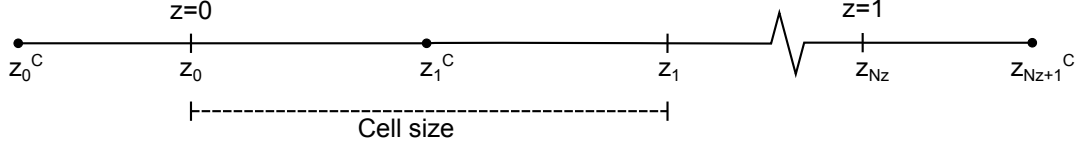


Figure 2.1: Schematic of the flow domain



**Figure 2.2:** Discretized domain in  $z$ -direction. Circle and line indicates cell center and cell face respectively.

This looks quite messy so we clean it up by multiplying with  $\frac{H}{\rho u_\tau^2}$  to get:

$$\frac{\partial u_i^*}{\partial t^*} + \frac{\partial u_i^* u_j^*}{\partial x_j^*} = -\frac{\partial p^*}{\partial x_i^*} + \frac{H}{\rho u_\tau^2} \frac{\mu u_\tau}{H^2} \frac{\partial^2 u_i^*}{\partial x_j^* \partial x_j^*} \quad (2.3)$$

It is easy to see that  $\frac{H}{\rho u_\tau^2} \frac{\mu u_\tau}{H^2} = \frac{1}{\text{Re}_\tau}$  and hence:

$$\frac{\partial u_i^*}{\partial t^*} + \frac{\partial u_i^* u_j^*}{\partial x_j^*} = -\frac{\partial p^*}{\partial x_i^*} + \frac{1}{\text{Re}_\tau} \frac{\partial^2 u_i^*}{\partial x_j^* \partial x_j^*} \quad (2.4)$$

For clarity,  $u_\tau = \sqrt{\tau_w/\rho}$ , is called friction velocity and it relates the wall shear stress to a velocity. Equation 2.4 is the non-dimensional form of Navier-Stokes solved in the DNS code, with  $\text{Re}_\tau = 360$ , a constant pressure gradient  $-dp^*/dx^* = 2$ , no-slip condition at the wall and periodic boundary conditions at the remaining directions.

## 2.2 Discretization Schemes

The turbulent flow studied in this thesis is homogeneous in streamwise and spanwise directions, and therefore a pseudospectral method is applied. The Navier-Stokes equations are solved using Fourier transforms in the homogeneous directions, while a second order staggered finite difference method is applied in wall normal direction.

### Domain Discretization

The domain is discretized by a uniform grid in streamwise and spanwise directions, where the cell sizes are given by  $\Delta x = 2\pi/N_x$  and  $\Delta y = \pi/N_y$ , where  $N_x$  and  $N_y$  are the number of grid points. In the wall normal direction the cell size is stretched by a harmonic continuous function yielding finer grid resolution near the walls, see figure 2.2. In other words the location of cell faces are given by the vector function:

$$\vec{z}(\vec{k}, s) = \frac{1}{2} \frac{\arctan(s(\vec{k} - \frac{1}{2}))}{\arctan(s\frac{1}{2})} + \frac{1}{2} \quad (2.5)$$

Where  $s$  is a stretching factor and  $\vec{k} = [0, 1, 2, \dots, N_z]/N_z$ , which means that the cell size in wall normal direction is given by:

$$\Delta z_i = z(k_i) - z(k_{i-1}) \quad \text{for} \quad i = 1, 2, \dots, N_z \quad (2.6)$$

Streamwise and spanwise velocities together with the pressure field are calculated at the cell center, which we define as:

$$z_i^C = \frac{1}{2}(z_i + z_{i-1}) \quad \text{for} \quad i = 1, 2, \dots, N_z \quad (2.7)$$

while the wall-normal velocities are calculated at the face of the cell.

### Spatial derivatives - wall normal direction

A second-order central difference scheme is chosen in wall normal direction, giving a first-order accuracy on a non-uniform grid. All derivatives of cell centered properties are defined at the cell faces and opposite, i.e. :

$$\frac{d}{dz} u_i^F = \frac{u_{i+1}^C - u_i^C}{z_{i+1}^C - z_i^C} \quad \frac{d}{dz} u_i^C = \frac{u_i^F - u_{i-1}^F}{z_i^F - z_{i-1}^F} \quad (2.8)$$

The derivation of second-derivatives is successive use of the above equations. If a property saved at a cell face is needed at the cell center, the interpolation scheme is simply the arithmetic mean.

$$u_i^F = \frac{1}{2}(u_{i+1}^C + u_i^C) \quad u_i^C = \frac{1}{2}(u_i^F + u_{i-1}^F) \quad (2.9)$$

### Spatial derivatives - homogeneous directions

The pseudospectral method implies that the derivatives in the homogeneous directions are calculated by means of Fourier transformations. The variables are transformed from physical space and into the spectral space where the calculations of derivatives are easier and much more accurate. Consider the velocity vector  $\vec{u}$

$$\vec{u}(\vec{x}, t) = \sum_k \vec{u}_k(t) e^{i\vec{k}\vec{x}} \quad (2.10)$$

where  $\vec{x} = [x, y, z]$  is the position vector in physical space and  $\vec{k} = [k_x, k_y, z, t]$  is the wave number vector in spectral space. Derivation of the transformed variable is simply done by multiplying with  $i\vec{k}$ , where  $i$  is the imaginary number. Hence the first and second derivative of  $\vec{u}$  in the streamwise direction is

$$\frac{d}{dx} \vec{u}(\vec{x}, t) = \sum_k \vec{u}_k(t) i\vec{k}_x e^{i\vec{k}\vec{x}} \quad \frac{d^2}{dx^2} \vec{u}(\vec{x}, t) = - \sum_k \vec{u}_k(t) \vec{k}_x^2 e^{i\vec{k}\vec{x}} \quad (2.11)$$

After the derivatives are calculated and the system of equations is solved, the terms are transformed back to physical space.

### Temporal Discretization

An explicit second-order accurate Adams-Bashforth scheme [7] is used for time-stepping/time integration.

$$y_{n+2} = y_{n+1} + h\left(\frac{3}{2}f(t_{n+1}, y_{n+1}) - \frac{1}{2}f(t_n, y_n)\right) \quad (2.12)$$

If we apply this to the Navier-Stokes equations we get [14]

$$\frac{\bar{u}^{n+1} - \bar{u}^n}{\Delta t} = \frac{3}{2}T(\bar{u}^n) - \frac{1}{2}T(\bar{u}^{n-1}) - \Delta p^{n+1} \quad (2.13)$$

with  $T(\bar{u}^n) = -(\bar{u}^n \cdot \nabla)\bar{u}^n + \text{Re}_*^{-1}\nabla^2\bar{u}^n$ . We know every value at time step  $n$ , hence we only have two unknowns;  $\bar{u}^{n+1}$  and  $p^{n+1}$ . Next we solve equation 2.13 without the pressure term, yielding a temporary value for the velocity,  $\bar{u}_*$ .

$$\frac{\bar{u}_* - \bar{u}^n}{\Delta t} = \frac{3}{2}T(\bar{u}^n) - \frac{1}{2}T(\bar{u}^{n-1}) \quad (2.14)$$

The lower index star indicates an intermediate value and must not be confused with  $\bar{u}^*$  indicating a non-dimensional value. If we subtract equation 2.14 from equation 2.13 we get

$$\bar{u}^{n+1} - \bar{u}_* = -\Delta t \nabla p^{n+1} \quad (2.15)$$

Now consider the divergence of this equation

$$\nabla \cdot \bar{u}^{n+1} - \nabla \cdot \bar{u}_* = \Delta t \nabla^2 p^{n+1} \quad (2.16)$$

In order to satisfy continuity  $\nabla \cdot \bar{u}^{n+1}$  must equal 0, resulting in a Poisson equation for the pressure

$$\nabla^2 p^{n+1} = \frac{\nabla \cdot \bar{u}_*}{\Delta t} \quad (2.17)$$

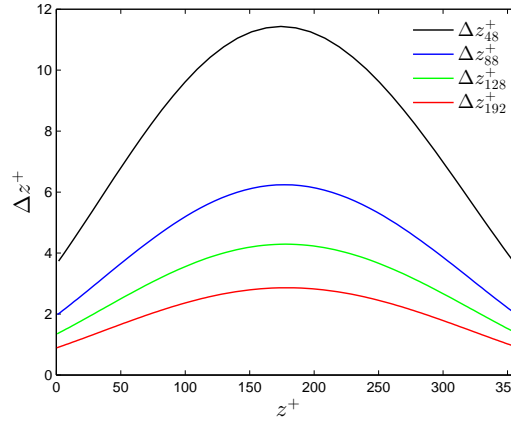
Equation 2.17 is solved using fast Fourier transforms, and can then be used to find the velocity at the new time step by going back to equation 2.16.

## 2.3 Grid Resolution

In this thesis four different grid resolutions and their impact are investigated. The resolutions used are  $48^3$ ,  $88^3$ ,  $128^3$  and  $192^3$  resulting in 110 592, 681 472, 2 097 152 and 7 077 888 number of cells respectively. In table 2.1 the <sup>+</sup>-superscript indicates a non-dimensional wall distance, i.e a quantity scaled by wall variables;  $y^+ \equiv yu_\tau/\nu = y\frac{u_\tau H}{\nu H} = \frac{y}{H}Re_\tau$ , with  $Re_\tau = 360$ . If we compare the  $192^3$  grid with data from [9] where  $\Delta y^+$  varies between 0.1 and 4.4, it is apparent that Kim et al.



Grid Size	$\Delta x^+$	$\Delta y^+$	max $\Delta z^+$	min $\Delta z^+$
$48^3$	47.12	23.56	11.43	3.73
$88^3$	25.70	12.85	6.24	1.98
$128^3$	17.67	8.84	4.29	1.35
$192^3$	11.78	5.89	2.86	0.89

**Table 2.1:** Grid properties by wall scaled quantities**Figure 2.3:**  $\Delta z^+$  for different grid resolutions

has employed a larger stretching factor in the wall normal direction giving a finer near-wall resolution but at the cost of mid-channel resolution. Because of large gradients near the wall this resolution is believed to be of critical importance to the quality of the simulation. The computational time was about  $10^{-2}$  s per time step for the  $48^3$  grid and 3 s per time step for the  $192^3$  grid. The cell size in the  $z$ -direction for the different cases, shown in figure 2.3 increases steadily with a larger jump from  $N_z = 88$  to  $N_z = 48$ .



# Chapter 3

## Results - Turbulence Statistics

After reaching a statistically steady velocity field the simulation is integrated further in time in order to gather representative time and space averaged properties. In space the quantities are of course only averaged in the homogeneous directions. Figure 3.1 illustrates the need for averaged values when dealing with turbulent flows. The randomness and chaotic structure of the velocity field makes the instantaneous values almost useless for comparison between cases as the strength of the perturbations are so high. However, when time averaging the velocity field becomes symmetric, predictable and suitable for comparisons, it will at a first glance resemble the velocity field of a laminar flow. The data presented in this chapter is compared with data from the 1987 article *Turbulence statistics in fully developed channel flow at low Reynolds number* by Kim, Moin and Moser [9]. Their data is thoroughly verified with experimental data and is considered correct by peers.

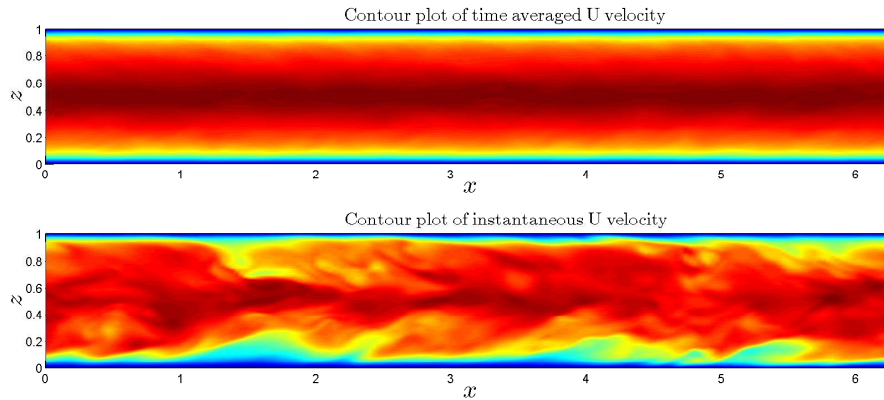


**Figure 3.1:** A comparison of a time averaged and an instantaneous velocity field

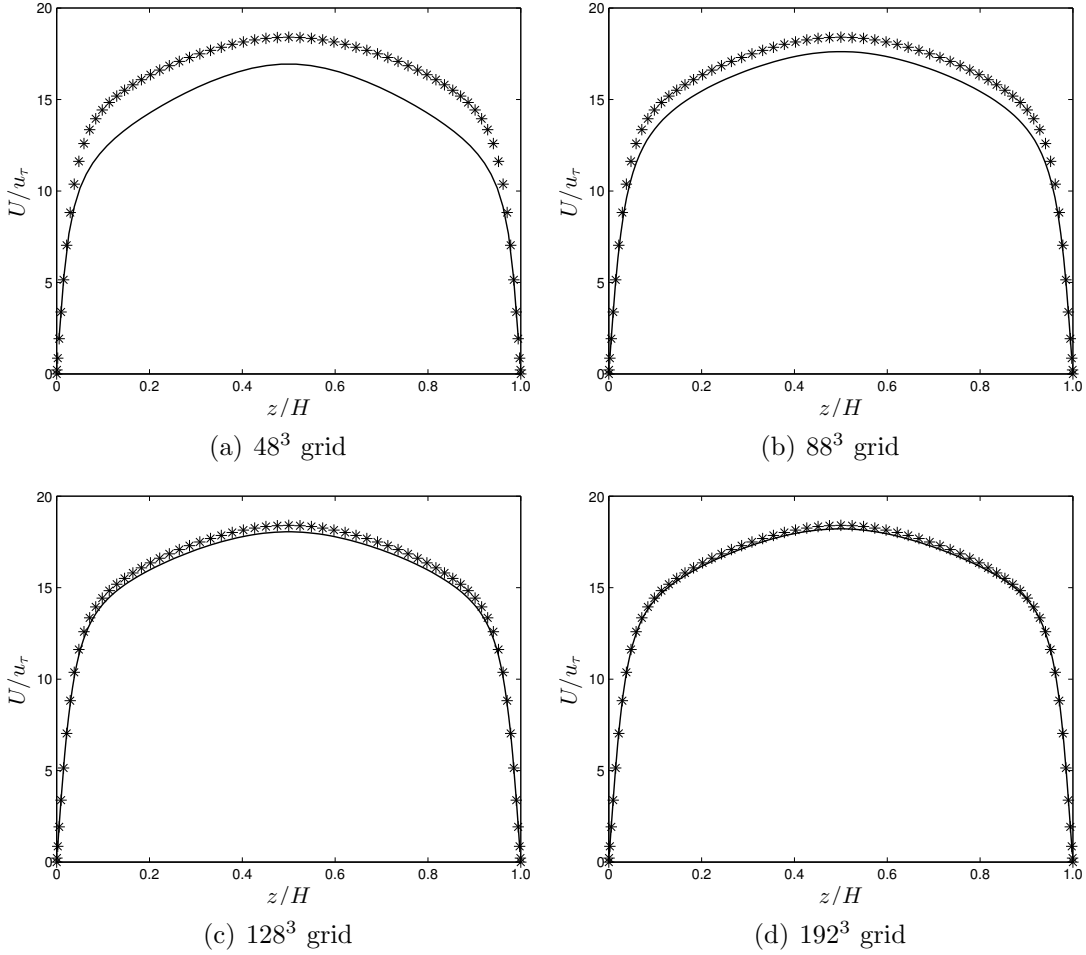


**Figure 3.2:** Mean velocity profile for the different grid resolutions compared with data from Kim et al. [9]

### 3.1 Mean Flow Properties

Figure 3.2 shows the evolution of the mean velocity profile as the grid resolution increases. The mean velocity profile moves towards a greater maximum and “flatter” curvature near the channel center, i.e.  $dU/dz$  moves closer to zero in this region. Compared with data from Kim et al. the difference in centerline mean velocity is 10.1% for the  $48^3$  grid and 0.58% for the  $192^3$  grid. The difference in bulk mean velocity normalized by  $u_\tau$  is 10.1% for the  $48^3$  grid and 0.064% for the  $192^3$  grid. The bulk mean velocity is defined as

$$U_m = \frac{1}{H} \int_0^H U dz \quad (3.1)$$

Figure 3.3 is a zoomed in view of the near wall region of the mean velocity profile

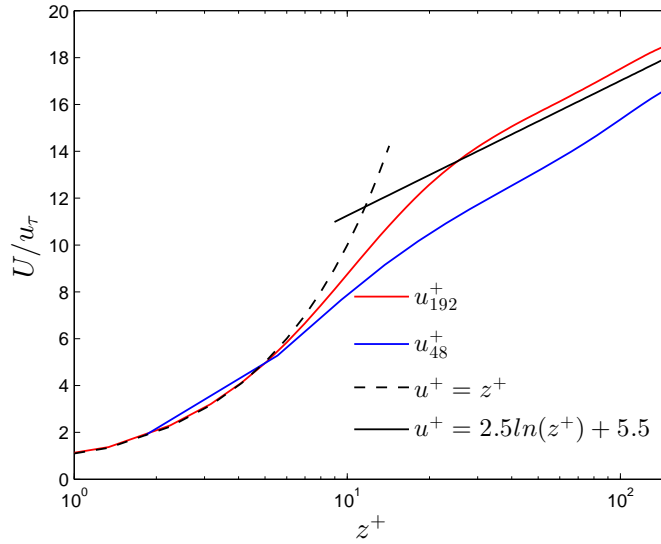


**Figure 3.3:** A closer look at the near wall mean velocity profiles for the coarsest and finest grid compared with the law of the wall

from figure 3.2. The two equations in the figure are derived from the law of the wall and describes velocity development in the viscous sublayer and the logarithmic layer. The law of the wall states that the normalized velocity is a function of the normalized wall distance, i.e.  $u^+ = f(z^+)$ , and more specifically:

$$f(z^+) = \begin{cases} z^+ & \text{if } z^+ < 5 \\ \frac{1}{\kappa} \ln(z^+) + B & \text{if } z^+ > 30 \end{cases} \quad (3.2)$$

The von Kármán constant,  $\kappa$ , and  $B$  are the same as given by [9] and [1]. See [6] for more details on the subject. The profile from the  $192^3$  grid shows excellent agreement with the law for  $z^+ < 5$  and good agreement for  $z^+ > 30$ , whilst the profile from the  $48^3$  grid seems to be almost logarithmic through all the layers. From figures 3.2 and 3.3 it is apparent that only the two finest grid resolutions,  $128^3$  and  $192^3$  are sufficiently accurate with regards to mean velocity profiles, although the  $88^3$  grid is surprisingly close.

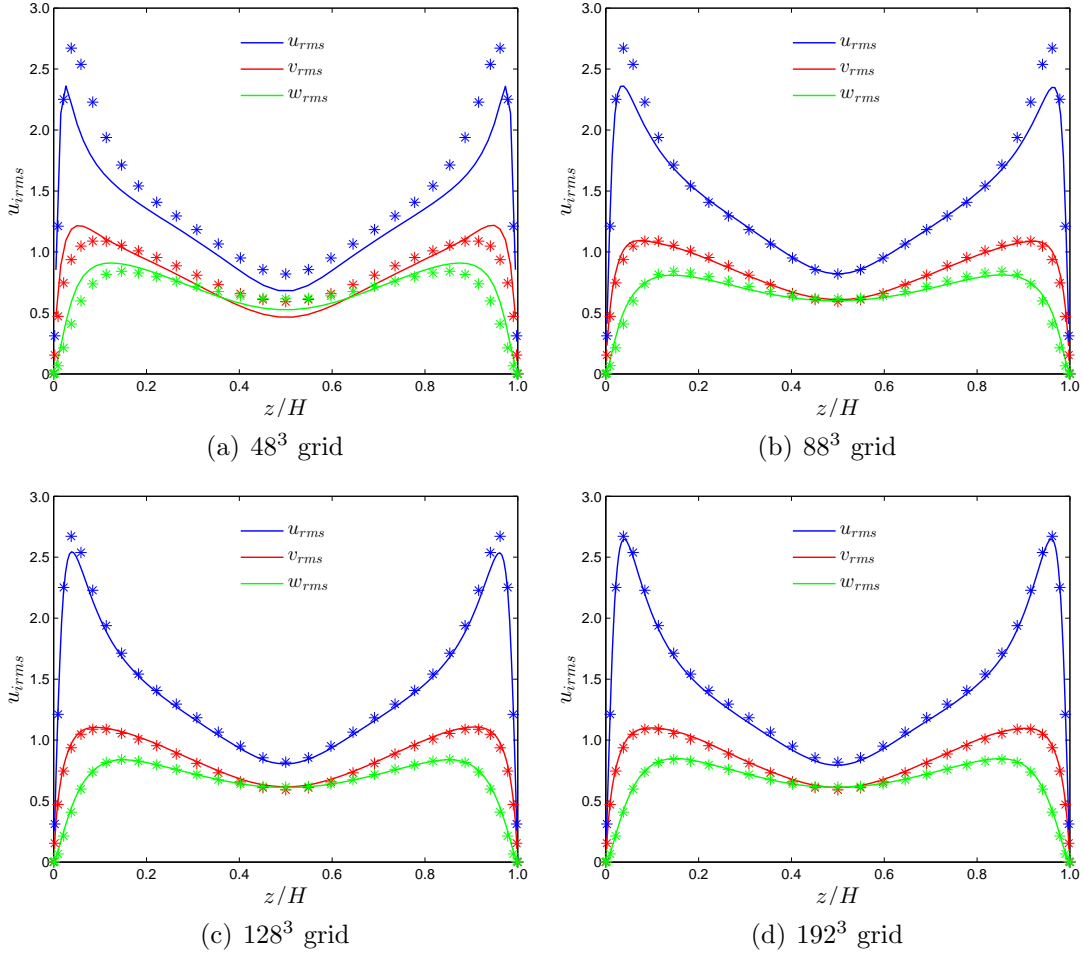


**Figure 3.4:** Root mean squared of velocity components for the different grid resolutions compared with data from Kim et al. [9], normalized with  $u_\tau$

## 3.2 Turbulence Intensities

When studying the turbulent dissipation it is vital to have accurate values of the turbulence intensities, see figure 3.4, or velocity fluctuations, as the dissipation term is only dependent on their derivatives. The profiles of the velocity fluctuations are symmetric about the centerline for all grids, and the  $u$ -fluctuations converges towards the data from Kim as the grid resolution increase. All grids have a maximum value of  $u$ -fluctuations at a wall distance of  $z^+ \approx 14$ . For the  $48^3$  grid there is an abrupt change at the maximum value, and for the  $v$  and  $w$  fluctuations it over predicts the values near the wall and under predicts near the center. This will result in over predicted values of dissipation in the spanwise and wall normal direction, i.e  $\epsilon_{22}$  and  $\epsilon_{33}$ , because of too high values of the derivatives of the fluctuating velocities. The over prediction of the  $v$  fluctuations near the wall can also be observed for the  $88^3$  grid, but it has already at that resolution

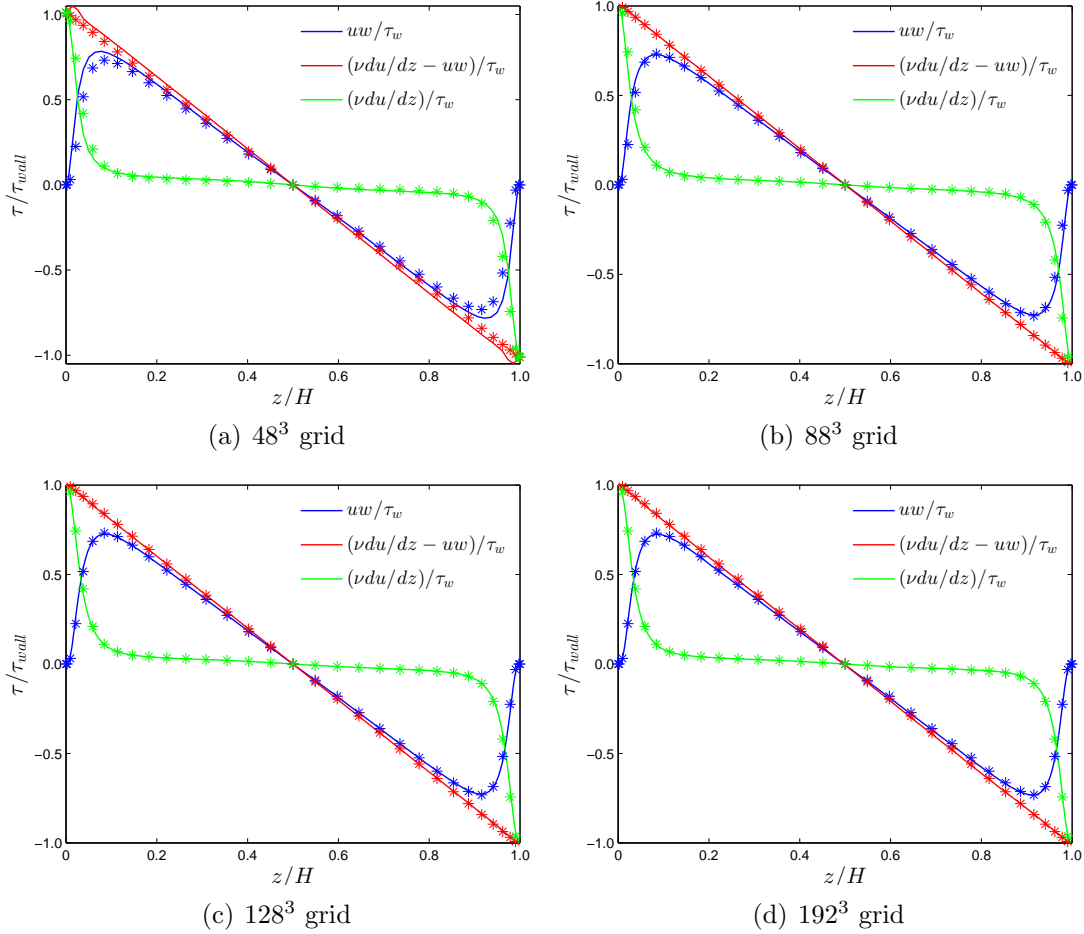


**Figure 3.5:** Shear forces for the different grid resolutions compared with data from Kim et al. (\*)

almost converged with the data from Kim.  $w$  fluctuations for the  $88^3$  is considered satisfactory. At the resolution of  $128^3$  the only fluctuation not converged is the  $u$  fluctuations, and it is only too low in the near periphery of the extrema. With grid resolution  $192^3$  the data agree everywhere with Kim.

### 3.3 Reynolds Shear Stress

Figure 3.5 shows the Reynolds shear stress in the flow, and the only grid resolution to give a notable discrepancy is the  $48^3$  grid. Since  $(\nu dU/dz)/\tau_w$  is almost exactly equal the data from Kim,  $\overline{uw}/\tau_w$  must be the inaccurate term.  $(\nu dU/dz)/\tau_w$  is closer to the data by Kim because it is only dependent on the shape of  $U_i(z)$  and not its magnitude, whilst  $\overline{uw}/\tau_w$  is of course dependent on the magnitude of  $U_i(z)$ .

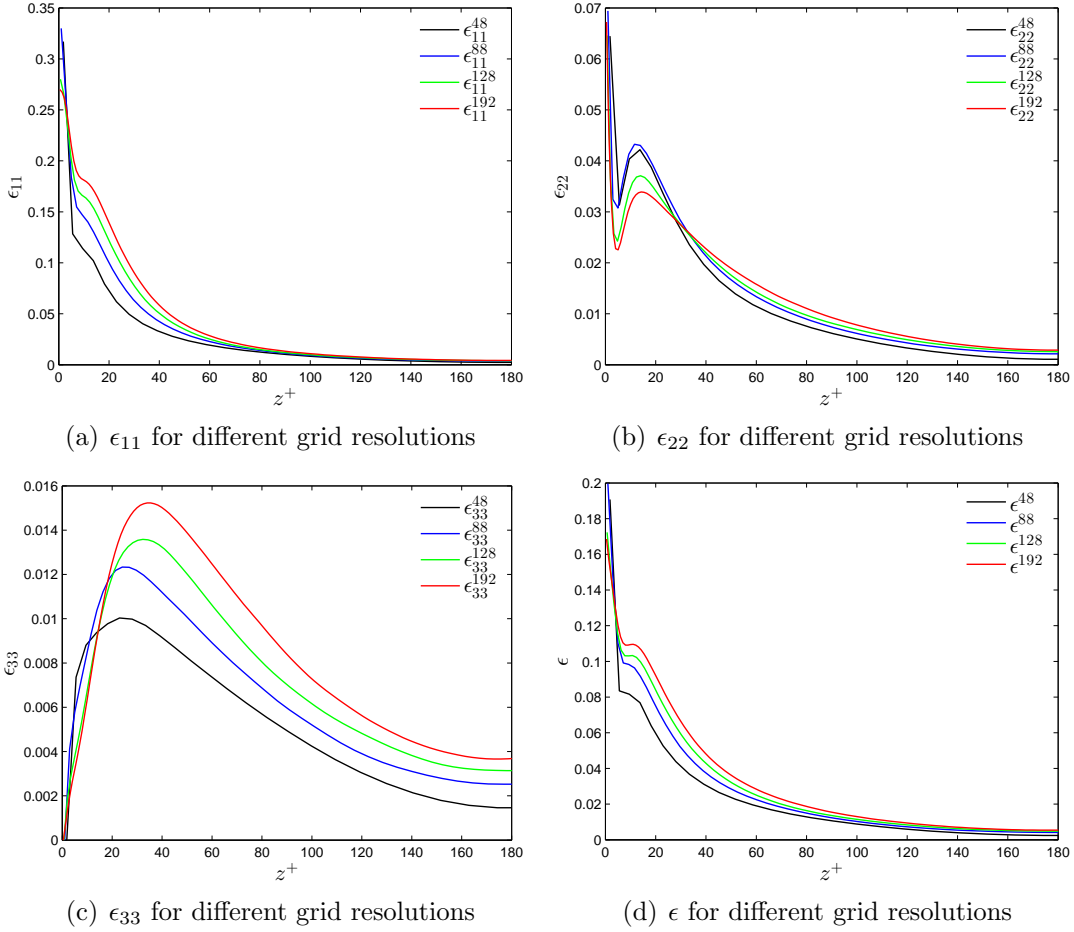


**Figure 3.6:**  $\epsilon_{11}$ ,  $\epsilon_{22}$ ,  $\epsilon_{33}$ , and  $\epsilon$  for different grid resolutions normalized by  $u_\tau^2/\nu$ . The superscript denotes grid resolution. No data from Kim available.

### 3.4 Turbulent Dissipation

Figure 3.6 shows the directional behavior of the turbulence dissipation. As expected, because of largest derivatives of the velocity fluctuations,  $\epsilon_{11}$  is the dominating term followed by  $\epsilon_{22}$  and  $\epsilon_{33}$ , and from equation 1.31

$$\epsilon = 0.5(\epsilon_{11} + \epsilon_{22} + \epsilon_{33})$$

hence has the shape of  $\epsilon_{11}$ . The amount of dissipation increases along with increased grid resolution for  $\epsilon_{11}$  and  $\epsilon_{33}$  but it decreases for  $\epsilon_{22}$ , and the only abnormality is seen with grid resolution  $48^3$  for  $\epsilon_{22}$ . Here we would expect  $\epsilon_{22}^{48}$  to have a larger value than  $\epsilon_{22}^{88}$  for  $z^+ \in [0, 36]$ , whereas the opposite is the fact. This discrepancy is caused by the over prediction of the fluctuating  $v$  and  $w$  velocity near the wall, which can easily be observed at low  $z$ -values for  $\epsilon_{33}$  where the dissipation has a steeper curve near the wall with decreasing grid resolution.



Here the derivative  $d\epsilon_{33}/dz$  decreases with increasing grid resolution as a direct result from the change seen between figures 3.4(a) and 3.4(d).

### 3.4.1 Homogeneous vs. Thermodynamical Dissipation

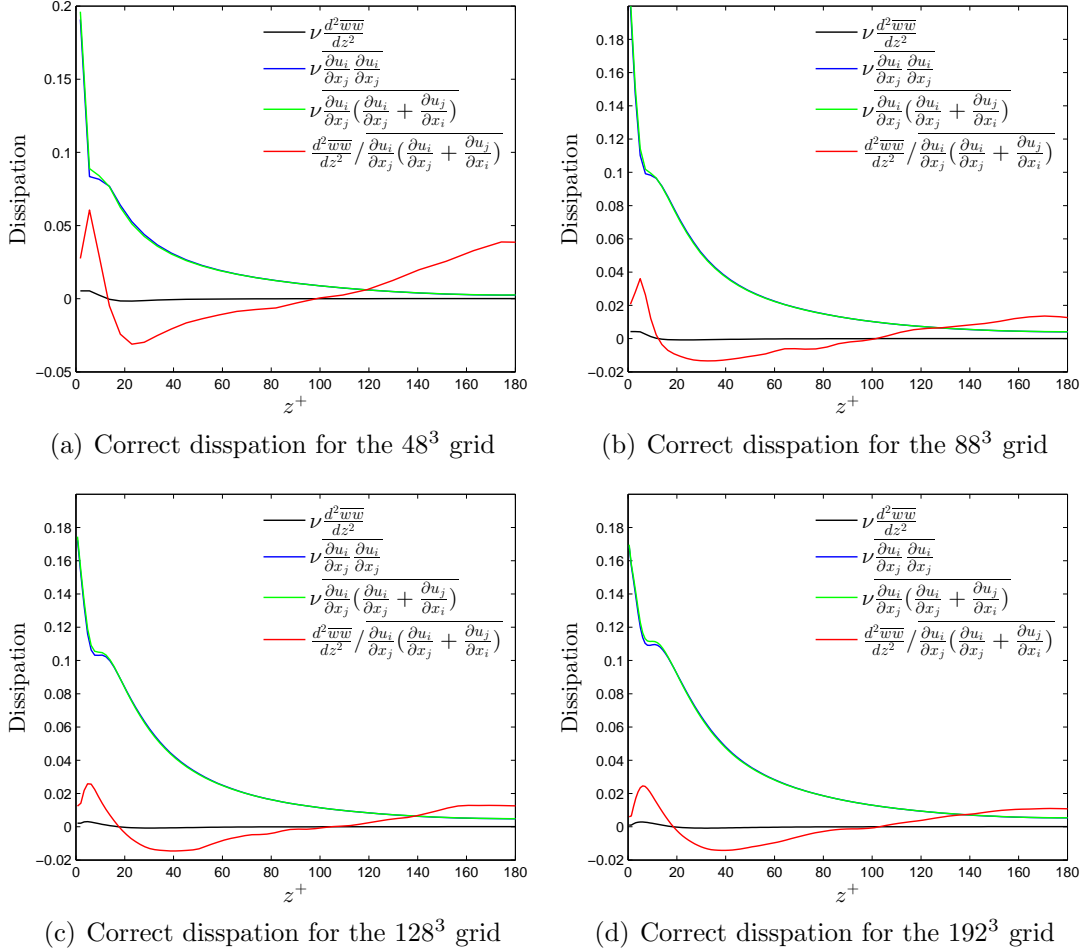


**Figure 3.7:** A comparison between the thermodynamic and homogeneous dissipation normalized by  $u_\tau^2/\nu$ , denoted by  $\epsilon$  and  $\epsilon$  respectively

To investigate the difference between the homogeneous dissipation and thermodynamically correct dissipation we look back at equations 1.21 and 1.24. These equations are as they appear in the note by Bradshaw and Perot [2], and the difference between the two dissipation terms is

$$\overline{\nu \frac{\partial u_i}{\partial x_j} \left( \frac{\partial u_i}{\partial x_j} + \frac{\partial u_j}{\partial x_i} \right)} - \overline{\nu \frac{\partial u_i}{\partial x_j} \frac{\partial u_i}{\partial x_j}} = \overline{\nu \frac{\partial^2 u_i u_j}{\partial x_i \partial x_j}} \quad (3.3)$$

Since this study is of a channel flow with homogeneous turbulence in streamwise ( $x$ ) and spanwise ( $y$ ) directions the term on the right hand side in equation 3.3 simplifies to

$$\frac{\overline{\partial^2 u_i u_j}}{\partial x_i \partial x_j} = \frac{d^2 \overline{w w}}{dz^2} \quad (3.4)$$

This term is compared with the exact dissipation by  $(d^2 \overline{w^2}/dz^2)/(\overline{\frac{\partial u_i}{\partial x_j} (\frac{\partial u_i}{\partial x_j} + \frac{\partial u_j}{\partial x_i})})$ , as shown in figure 3.7. Figure 3.7 shows that there is very little difference between the homogeneous and thermodynamic dissipation, in fact for the  $192^3$  grid the integrated difference is 0.14%, i.e.

$$\frac{\int_0^H \overline{\frac{\partial u_i}{\partial x_j} \frac{\partial u_i}{\partial x_j}} dz}{\int_0^H \overline{\frac{\partial u_i}{\partial x_j} (\frac{\partial u_i}{\partial x_j} + \frac{\partial u_j}{\partial x_i})} dz} = 0.9986 \quad (3.5)$$

For the  $128^3$  grid the difference is 0.18%, and it is 0.23% and 0.35% for the two coarsest resolutions of  $88^3$  and  $48^3$  respectively. So even if the viscous diffusion term is almost 2.5% of the thermodynamic dissipation at  $z^+ \approx 6$ , for the  $192^3$  grid, it does not affect the magnitude of the dissipation but rather acts as a redistribution term. The term adds to the dissipation near the wall until  $z^+ \approx 20$ , then it reduces dissipation until  $z^+ \approx 100$ , where it returns to add to the dissipation. The only “real” deviation between the correct and homogeneous dissipation is that the inflection point at  $z^+ \approx 9$  is no longer an inflection point. These results are in agreement with the findings of Bradshaw and Perot [2].

### 3.4.2 Homogeneous vs. isotropic dissipation

Figure 3.8 shows that the channel flow clearly is anisotropic, which we already knew from the velocity fluctuations. The homogeneous dissipation is plotted against isotropic dissipation given by equation 1.45. The implication of the wall boundary condition is apparent, and creates anisotropic turbulence for  $z^+ < 150$ , leaving only a small region about the channel center which can be said to be approximately isotropic. The  $192^3$  grid is used for the comparison.

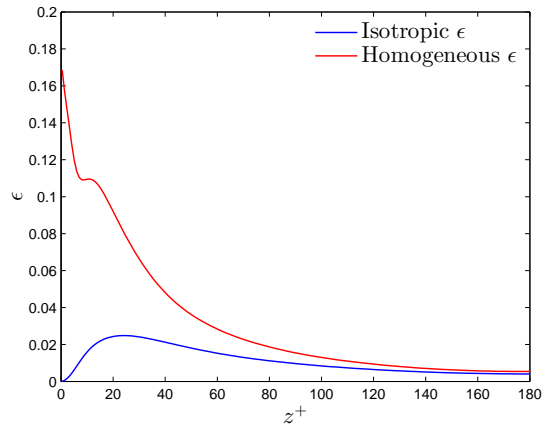
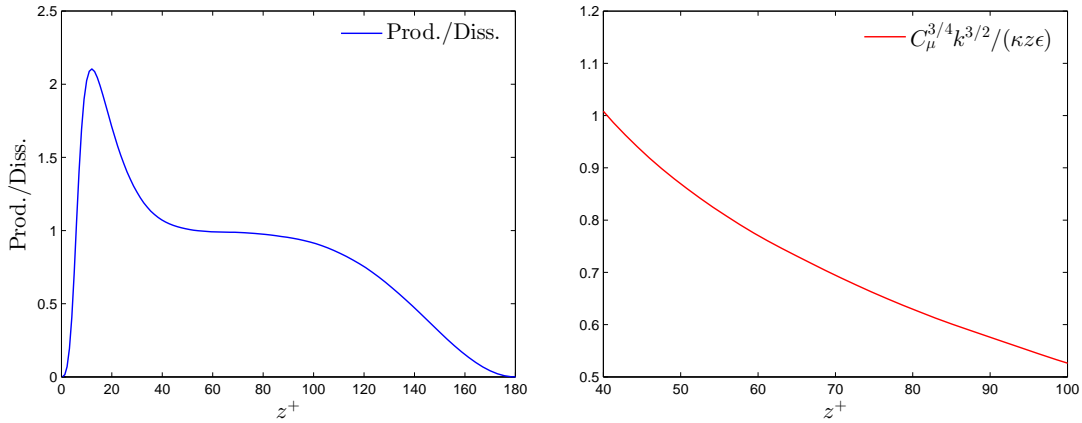


**Figure 3.8:** A comparison between isotropic and homogeneous dissipation



(a) Ratio of turbulent kinetic energy production to dissipation (b) Dissipation in  $k$ - $\epsilon$  model in log-law region, normalized by  $\epsilon$

**Figure 3.9:** Location of log-law region found from (a) and dissipation plotted in (b)

### 3.4.3 Dissipation in the $k$ - $\epsilon$ -Model

Figure 3.9(b) shows the dissipation calculated from equation 1.55 scaled by the homogeneous dissipation from the DNS simulation in the log-law region, identified by figure 3.9(a). The ratio goes from 1 for  $z^+ = 40$  to approximately 0.5 for  $z^+ = 100$ , but with large derivatives at both ends of the log-law layer.

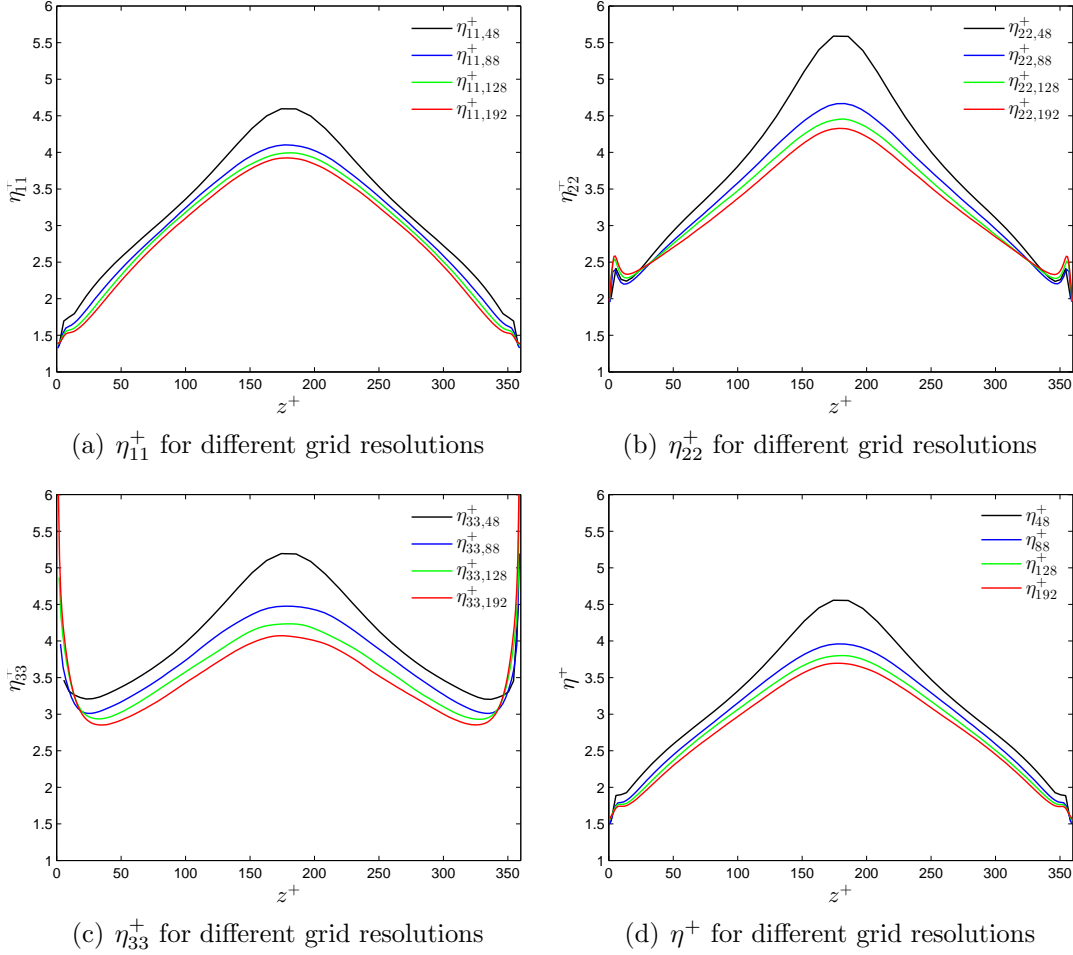


**Figure 3.10:** Kolmogorov length scale based on total dissipation and its components

### 3.5 Kolmogorov Length Scale

Figure 3.10 shows the Kolmogorov length scale,  $\eta^+$ , as a function of dissipation,  $\epsilon(z^+)$ . The length scales are decomposed by the corresponding dissipation terms, e.g.  $\eta_{11}^+ = f(\epsilon_{11})$  and  $\eta^+$  is calculated with  $\eta^+ = [\nu^3/(0.5\epsilon_{ii})]^{1/4}$ . Since the Kolmogorov length scales are dependent on the dissipation the components will naturally behave similarly to the reciprocal of the dissipation functions, with  $\eta_{11}^+$  giving the strongest impact on  $\eta^+$ ,  $\eta_{22}^+$  shows similar behavior while  $\eta_{33}^+$  separates from the other directions because of the wall condition. The Kolmogorov length scale increases a lot for the  $48^3$  grid around the center of the channel, this is due to  $\epsilon^{48}$  decreasing more than it “should”, relative to the other too coarse resolutions. The inflection point at  $z^+ \approx 9$  for the dissipation in figure 3.7 can be seen for the Kolmogorov length scales as well. For the  $48^3$  grid the global maximum of all components is  $\eta_{22}^+ \approx 5.6$ , while the global minimum is  $\eta_{11}^+ \approx 1.35$ . For the  $192^3$  grid the corresponding values are  $\eta_{22}^+ \approx 4.3$  and  $\eta_{11}^+ \approx 1.39$ . In general the

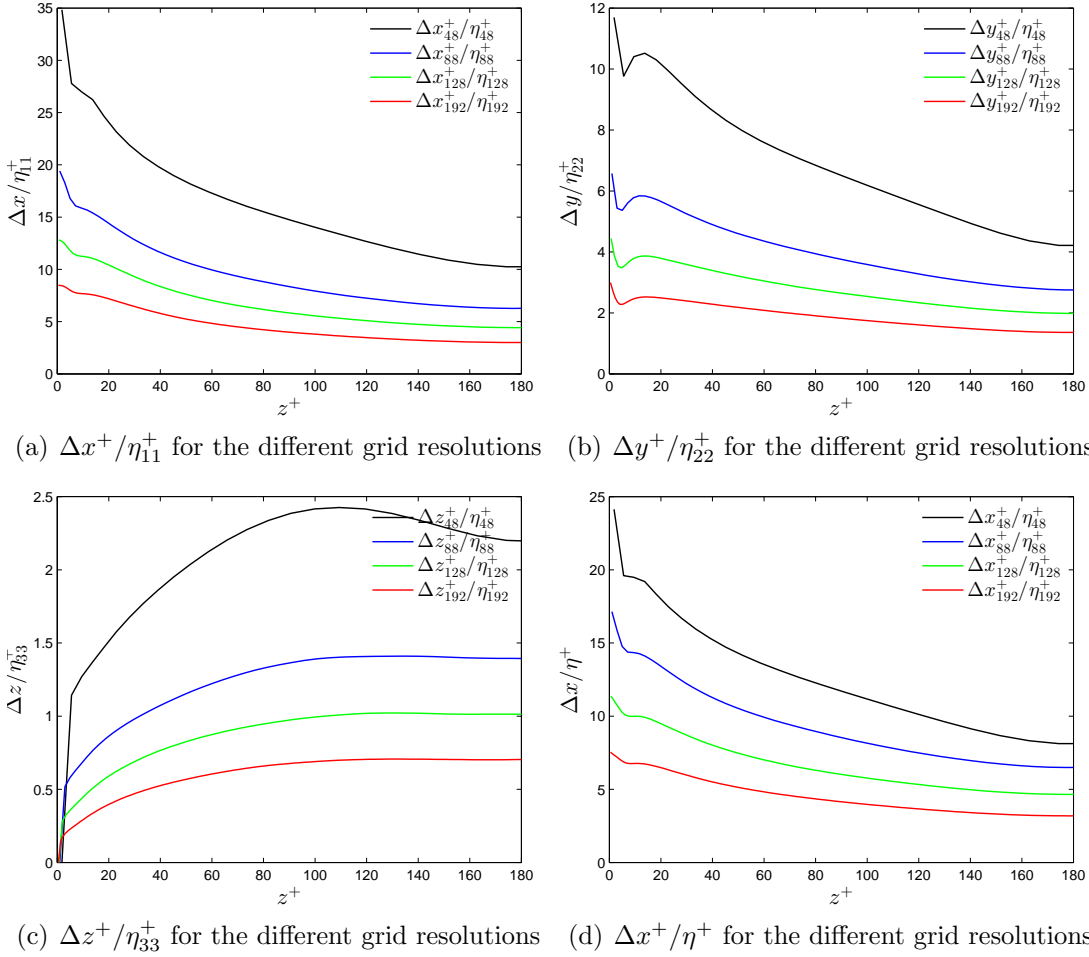


**Figure 3.11:** The ratio of cell size to the Kolmogorov length scale

Kolmogorov length scale decreases with increasing grid resolution because of the increase in dissipation.

Figure 3.11 shows the ratio of cell size to Kolmogorov length scale for the different components, note that it is the grid's own Kolmogorov length scale which is used. The difference between the cases is significant, ranging from a ratio of  $\Delta x/\eta_{11}^+ \approx 35$  for the  $48^3$  grid to  $\Delta x/\eta_{11}^+ \approx 3$  for the  $192^3$  grid, shown in figure 3.11(a). The only direction which has fully resolved the Kolmogorov length scale is the  $z$ -direction, where the  $192^3$  grid has a ratio of 0.7 and the  $128^3$  grid must also be considered as resolved with a ratio of 1.01.  $\Delta x$  is chosen for the comparison with  $\eta^+$ , see figure 3.11(d), because it is the largest cell size. Here the  $48^3$  grid goes from approximately 25 near the wall to 8 in the center, while the  $192^3$  grid varies between approximately 7.5 at the wall and 3 in the channel center. With a grid resolution of  $128^3$  the ratio is as much as about 11 near the wall.

Figure 3.12 shows the ratio of the geometric mean,  $\Delta$ , to the Kolmogorov

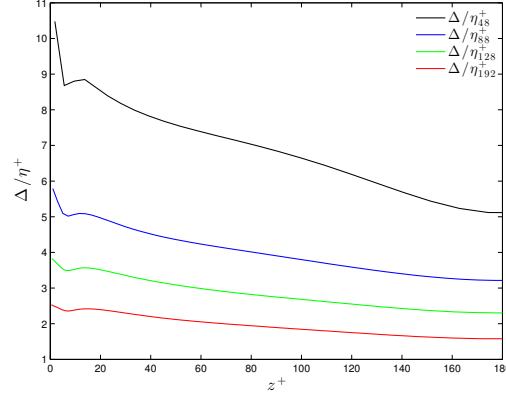


**Figure 3.12:**  $\Delta/\eta^+$  for different grid resolutions

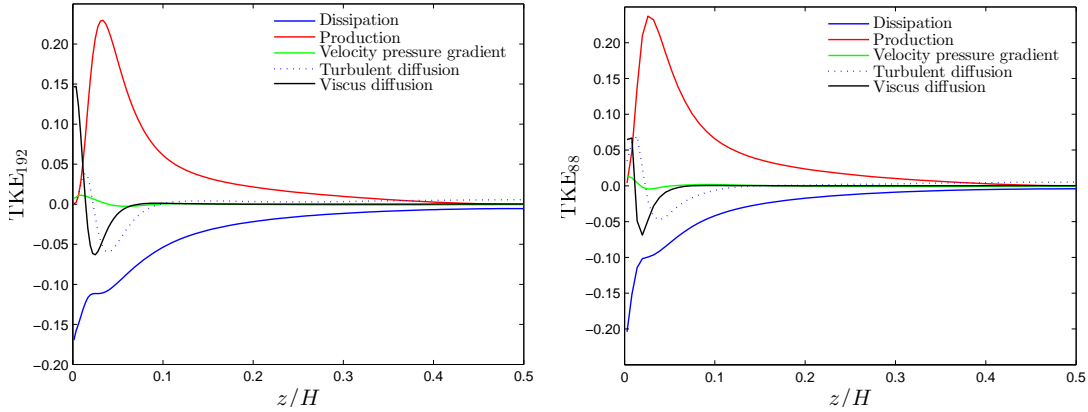
length scale. The geometric mean,  $\Delta = (\Delta x \Delta y \Delta z)^{1/3}$ , can be seen as a cubic length conversion of the volume of the computational cells, since it describes a cube with edge length  $\Delta$  with the same volume as the cell  $\Delta x \Delta y \Delta z$ . Applying  $\Delta$  instead of  $\Delta x$  reduces the ratio by approximately 3,

## 3.6 Turbulent Kinetic Energy Budget

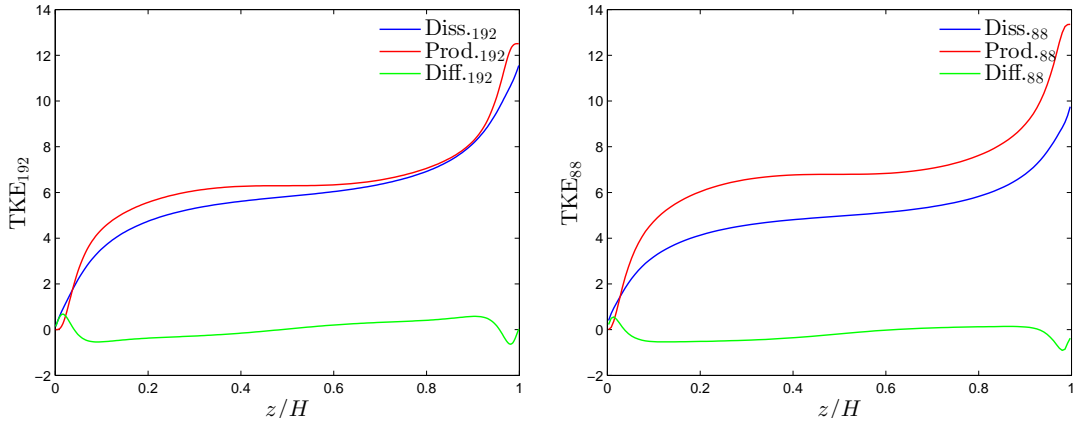
Figures 3.13(a) and 3.13(b) shows the turbulent kinetic energy budget and figures 3.13(c) and 3.13(d) the cumulative distribution of production, dissipation and diffusion in the  $z$ -direction for the two grid resolutions  $192^3$  and  $88^3$ . Since there exist a derivative of the mean velocity in the wall normal direction it is possible for the kinetic energy to be steady<sup>1</sup>, i.e.  $\overline{Dk/Dt}$  can and should be zero. This implies that the sum of the integrated energy budget is zero, and this added with the fact that diffusion terms integrated over a surface (for fully developed flow) are zero means that production should equal dissipation when integrated over a surface. Since the turbulence is homogeneous in streamwise and spanwise directions it is sufficient to integrate along a line in wall normal direction. For figures 3.13(c) and 3.13(d) the diffusion is the sum of turbulent diffusion, viscous diffusion and the velocity pressure gradient. The diffusion integrated from wall to wall for the  $192^3$  grid adds up to  $\approx 0.035$ , while the  $88^3$  grid resolutions gives a value of  $\approx 0.37$ , a ratio of  $\approx 10.6$ . The production shows less deviation with  $\approx 12.5$  and  $\approx 13.35$  for the  $192^3$  and  $88^3$  grid respectively, resulting in a ratio of  $\approx 1.07$ . Lastly, the dissipation goes from  $\approx 11.6$  to  $\approx 9.75$ , a ratio of  $\approx 0.84$ . Looking to figures 3.13(a) and 3.13(b) the data from  $192^3$  is in good agreement with Mansour et. al [13]<sup>2</sup>, except that the viscous diffusion is 13% lower than the dissipation at

<sup>1</sup>For homogeneous turbulence with no mean velocity gradients this is impossible as the dissipation then have to be zero, see equation 1.26.

<sup>2</sup>The data in [13] is based on KMM



(a) The turbulent kinetic energy budget with grid resolution of  $192^3$  (b) The turbulent kinetic energy budget with grid resolution of  $88^3$



(c) Cumulative distribution of the budget with grid resolution of  $192^3$  (d) Cumulative distribution of the budget with grid resolution of  $88^3$

**Figure 3.13:** The turbulent kinetic energy budget and its cumulative distribution

the wall, whereas they compute equal rate of dissipation and viscous diffusion. The dissipation at the wall,  $\epsilon_w = 0.1686$ , is 1.6% higher than the data from Mansour et. al. When  $z^+ < 5$  viscous diffusion behaves as the dissipation. For the  $88^3$  grid resolution the viscous diffusion is 68% lower than the dissipation.





# Chapter 4

## Discussion

Since the tasks given for this master thesis is given in a structured manner, it is convenient to apply a similar structure in the following discussion. This chapter begins with a discussion of the approximations of dissipation in experiments and turbulence models with basis in the theory given and results obtained. Then a discussion of the dissipation components follows, and how the homogeneous dissipation differ from the thermodynamical dissipation. After that attention is given to how grid dependency impacts the Kolmogorov length scale and the simulation accuracy. Lastly an investigation is made of the directional behavior of the Kolmogorov length scale, with an attempt to make a length scale tensor analogous to the Kolmogorov length scale.

### 4.1 Approximating Dissipation

#### Experiments

In the case of the approximation for the dissipation in experiments, i.e. equation 1.45, the word “approximation” is a bit ambiguous since the equation itself is exact. It is the assumptions behind its derivation, namely homogeneous and isotropic turbulence, which cause trouble as these flow properties are the exception rather than the rule. In low Reynolds number channel flow it is expected poor results from this approximation, which the results in figure 3.8 also show. It is possible that a higher Reynolds number would give a larger region about the centerline where the approximation would yield good results, but then the fluctuations near the wall would increase giving large discrepancies. There is however little doubt that this is a powerful approximation when utilized correctly, making experiments faster, easier and cheaper. It should be remembered that this is the most basic approximation, and more advanced expressions exist.

### Turbulence Models

With regards to the dissipation in the  $k$ - $\epsilon$ -model the comparison yielded little results, as the comparison was made with an anisotropic  $k$ , whereas a  $k$  calculated with the model would be isotropic. An effort has been made by the author into converting the anisotropic  $k$  to an isotropic  $k$ , but the the results were unsuccessful. It could be interesting to compare dissipation from a a proper calculation with the model with the DNS data.

## 4.2 Dissipation

As stated earlier in the theory chapter the dissipation of turbulent kinetic energy depends only on the gradients of the velocity fluctuations. These fluctuations are in the small scale and demands high grid resolutions to be resolved accurately, and the grid spacing should be at least equal to the Kolmogorov length scale in order to resolve every scale. At the same time most of the dissipation occurs at scales larger than the Kolmogorov length scale. Moser and Moin [15] found that most of the dissipation occurs at scales larger than  $15\eta$  for a curved channel, relaxing the grid size requirements some. Remember that the Kolmogorov scale is the *smallest* scale at which dissipation occurs.

### Dissipation Components

The results for dissipation of turbulent kinetic energy shows that the dissipation rate increases with increasing grid resolution, which makes sense from the arguments above. Following this logic the dissipation thus converge towards a finite amount with increasing resolution. Through the Reynolds stress equations the dissipation is separated into components representing the streamwise, spanwise and wall-normal directions. The most predominant component is the streamwise  $\epsilon_{11}$ , dictating the behavior of the scalar dissipation. Since  $\epsilon_{11} > \epsilon$  the components do not make much physical sense, i.e. the streamwise dissipation rate can not be larger than the total dissipation rate in all directions, but they can perhaps be utilized to create a tensor-version of the Kolmogorov length scale which will be discussed later. By closer inspection of the near-wall behavior it becomes clear that the overshoot of the lower resolutions is due to  $\epsilon_{11}$ .  $\epsilon_{33}$  also over predicts near the wall for the lower resolutions, and for this component the whole curve seems to be skewed towards the wall. Opposed to the other two components,  $\epsilon_{22}$  shows a maximum value for the lower resolutions for  $z^+ \approx 15$ .

### Homogeneous and Thermodynamically Correct Dissipation

Bradshaw and Perot found that the assumption of homogeneous dissipation is accurate for all practical purposes, which also is the conclusion to be made from

the results in this thesis. The term which makes the difference between homogeneous dissipation and the correct dissipation is the viscous diffusion term,  $\frac{\partial^2 \overline{u_i u_j}}{\partial x_i \partial x_j}$ , which with the divergence theorem gives

$$\int_V \frac{\partial^2 \overline{u_i u_j}}{\partial x_i \partial x_j} dV = \int_A n_i \frac{\partial \overline{u_i u_j}}{\partial x_j} dA = \int_{-H/2}^{H/2} \frac{d\overline{w\overline{w}}}{dz} b dz = b \left[ \overline{w\overline{w}} \right]_{-H/2}^{H/2} = 0 \quad (4.1)$$

because of the wall boundary condition and homogeneity in streamwise and spanwise directions, and  $b$  is the breadth of the integrated surface. The reasons for this term not being exactly zero in the results could be insufficient sampling time for the time averaging, creating asymmetric distribution or numerical error as the wall-normal direction is only first order accurate. As the equation show there is no change made by the viscous dissipation term if it is integrated over a volume, it will however redistribute the dissipation rate within the volume. It is found that it gives a maximum increase of 2.5% at  $z^+ \approx 7$  compared to the homogeneous dissipation, and a maximum reduction compared to the homogeneous dissipation of 1.14% at  $z^+ \approx 40$ . Thus the effect of the viscous dissipation term is a reduction of the dissipation rate in  $18 < z^+ < 105$  and consequently an increase for the remaining  $z^+$  values.

### Turbulent Kinetic Energy Budget

The figures showing the cumulative distribution of turbulent kinetic energy production, dissipation and diffusion reveals that the  $192^3$  simulation is good, but not perfect. Both the diffusion and the difference between production and dissipation should add up to zero. From the discussion of dissipation it is concluded that dissipation increases with increasing grid resolution as the grid approaches the Kolmogorov length scale, but the figures of TKE show that production increases with decreasing grid resolution. Hence lowering the grid resolution results in a “double” punishment, as production and dissipation moves in opposite directions. The production term consist of the second moment of fluctuating velocity and the mean velocity gradient, i.e.  $\overline{u_i u_j} dU/dz$ , and a simple order of magnitude analysis will show that the dominating term is the mean velocity gradients. The dissipation however consist of the gradients of the velocity fluctuations, which requires much higher grid resolution, and that explains why the production reacts less than the dissipation towards decreasing grid resolution.

## 4.3 Kolmogorov Length Scale

The computed Kolmogorov scales in section 3.5 shows that a grid is capable of reporting the Kolmogorov scale to be less than its own grid size, though it is not grid independent. For example the coarsest  $48^3$  grid has minimum cell sizes  $(\Delta x^+, \Delta y^+, \Delta z^+) = (47.1, 23.6, 3.7)$  while the minimum computed Kolmogorov

length scale is  $\eta^+ \approx 1.53$ . All grids compute approximately the same  $\eta^+$  at the wall, and the largest difference between the grids is where the dissipation rate is lowest. The reason for this is that the fractional difference becomes great for small values, and with

$$\frac{\eta_1}{\eta_2} = \left( \frac{\epsilon_2}{\epsilon_1} \right)^{1/4} \quad (4.2)$$

it is clear that the center region of the channel will show the largest differences in Kolmogorov length scale. Compared with  $\eta_{192}^+$ ,  $\eta_{128}^+$  is 2.8% larger,  $\eta_{88}^+$  is 7.2% larger and  $\eta_{48}^+$  is 23.4% larger. Based on the averaged dissipation across the channel height the Kolmogorov length is 2.36 for the  $192^3$  grid, and based on the averaged production the Kolmogorov length is 2.31. Since the dissipation rate increases with grid resolution, production decreases and the Kolmogorov scale behaves opposite it is probable that the averaged Kolmogorov length scale is somewhere between 2.31 and 2.36.

### Grid Comparison

Figure 3.11 in previous chapter shows the different grid sizes compared to the Kolmogorov length scale. As stated before, to resolve everything these functions should have a maximum value of 1. The only grids to have such fine resolution are the  $128^3$  and  $192^3$  grids, and that is only for  $\eta_{33}^+$ , but those grids both have  $\Delta x_i^+ < 15\eta^+$  everywhere. They should then by the conclusion of Moser and Moin capture the bulk of the dissipation, but integrated from wall to wall the dissipation rate of the  $128^3$  grid is 7.8% less than that of the  $192^3$  grid. Almost 10% must be considered a large difference and hence for the case of low Reynolds number channel flow the “rule of thumb” from Moser and Moin, section 4.2, is quite inaccurate. The continuing change of the scale shows that there is still inaccuracies in the simulation, and a better simulation is possible.

### Directional Behavior

The directional behavior of the Kolmogorov scale is based on the Reynolds stress dissipation rate components and hence similar in its behavior. The Kolmogorov length scale is therefore smallest in the streamwise direction and increasing in spanwise and wall-normal direction. In the wall-normal direction,  $\eta_{33}^+$ , where the cell sizes for  $128^3$  and  $192^3$  are equal or less than the Kolmogorov scale there still is grid dependency. The reason for this change, even though it is “supposed” to be resolved, is probably because  $\epsilon_{33}$  is dependent on the  $x$ ,  $y$  and  $z$  derivatives of the fluctuating  $w$  velocity. So if the  $x$  and  $y$  directions are not resolved, with a grid improvement they will affect  $\epsilon_{33}$  even though the  $z$ -direction was already resolved. This could be confirmed or rejected by running a fully resolved simulation in all but one direction, and then increase resolution in that direction and compute the changes.

### Length Scale Tensor

It is proposed a length scale tensor, or specifically a vector, which relates the Kolmogorov length scale to the components in the Reynolds stress tensor.

$$\boldsymbol{\eta} = \alpha \left[ \left( \frac{\nu^3}{\epsilon_{11}} \right)^{1/4}, \left( \frac{\nu^3}{\epsilon_{22}} \right)^{1/4}, \left( \frac{\nu^3}{\epsilon_{33}} \right)^{1/4} \right] \quad (4.3)$$

There are however some issues with this length scale vector. For instance the Reynolds stress dissipation component in the streamwise direction is larger than the turbulent kinetic energy dissipation, perhaps making the grid restriction too strict. Therefore a scaling parameter,  $\alpha$ , is introduced. Since the dissipation rate of turbulent kinetic energy is given by half the trace of the Reynolds stress dissipation, the dissipation of kinetic energy, e.g. in the  $x$ -direction, can be given as  $\epsilon_{k,x} = 0.5\epsilon_{11}$ . This suggest a scaling parameter  $\alpha = 2^{1/4} \approx 1.2$ , and relaxes the grid restrictions compared with using the Reynolds stress dissipation as well as the restriction from the Kolmogorov length scale. Whether this length scale tensor is strict enough or not was not possible to investigate during this thesis, as the super computer was unavailable.

## 4.4 Further Work

- Due to the lack of computing power some tasks had to be omitted, e.g. simulation of grid resolution  $256^3$ . It is proposed to run a grid of  $256^3$  or higher, and compare that with  $256 \times 256 \times (192 \text{ or } 128)$ . Since the  $z$ -direction is resolved for the  $192^3$  grid is interesting to see the change between  $256^3$  and  $256 \times 256 \times 192$ .
- More stretching in the grid could be employed to give finer resolution near the wall.
- Utilizing the proposed length scale vector together with average dissipation across the channel height, the corresponding grid becomes  $[\Delta x^+, \Delta y^+, \Delta z^+] = [3.1, 4.2, 4.7]$ . This suggest a cell distribution of  $\approx (700, 300, 100)$  in  $x$ ,  $y$  and  $z$ -direction respectively. If the suggestion in the first point, shows no grid dependency when there are 192 cells in the  $z$ -direction, the grid proposed here could be interesting.
- Implementation of a higher order accuracy scheme in wall-normal direction.

## 4.5 Conclusion

The turbulence statistics presented are in good agreement with the data from Kim et al. [9] for grid resolution of  $192^3$ , however the dissipation data was not available and thus not compared. The dissipation was found to increase along with the grid resolution, and in agreement with Bradshaw and Perot [2] the extra viscous term in the correct dissipation term is a maximum of almost 2.5% of the correct dissipation term. The dissipation increases as the grid resolution approaches the Kolmogorov length scale. It is concluded that a simulation with higher resolution has to be made to be certain that the results are grid independent, although the dissipation at the wall agrees well with that reported by Mansour et al. [13].

The isotropic dissipation roughly agrees about the centerline of the channel, and the comparison with the  $k$ - $\epsilon$ -model is mostly made as a curiosity and has no practical value for this thesis.

Since the dissipation was found to be grid dependent, then ipso facto the Kolmogorov length scale is grid dependent. It is therefore difficult to draw any conclusions based on the results, other than that the grid can calculate Kolmogorov length scales smaller than the grid size itself. The wall-normal direction is resolved with respect to the Kolmogorov length scale, so the grid dependency is most likely because of the resolution in spanwise and streamwise direction for the  $192^3$  grid.

The components of the energy dissipation tensor presented are used to investigate the directional behavior of the Kolmogorov length scale. In streamwise direction the Kolmogorov length scale is smaller than the scale calculated from the scalar dissipation, and it is larger in spanwise and wall-normal direction. On the basis of the connection between the Reynolds stress equation and the equation for turbulent fluctuating kinetic energy it is proposed a length scale vector, analogous to the Kolmogorov length scale. This length scale vector gives a slightly higher value for the scales than the Kolmogorov scale, but unfortunately it was not possible to run any simulation to test its implications due to the lack of computing power.

# Bibliography

- [1] J. Anderson and J. Wendt. *Computational fluid dynamics*, volume 206. McGraw-Hill, 1995.
- [2] P. Bradshaw and J. Perot. A note on turbulent energy dissipation in the viscous wall region. *Physics of Fluids A: Fluid Dynamics*, 5:3305, 1993.
- [3] M. Chopra and B. Uensal. Hot wire anemometry and fluid flow measurement. <http://www.leb.eei.uni-erlangen.de/winterakademie/2008/report/content/course01/pdf/0107.pdf>, 2012. Indian Institute of Technology Delhi.
- [4] S. Corrsin. Interpretation of viscous terms in the turbulent energy equation. *J. Aeronaut. Sci.*, 12:853–854, 1953.
- [5] L. Davidson. Fluid mechanics, turbulent flow and turbulence modeling. [http://www.tfd.chalmers.se/~lada/MoF/lecture\\_notes.html](http://www.tfd.chalmers.se/~lada/MoF/lecture_notes.html), March 2012.
- [6] W. George. Is there a universal log law for turbulent wall-bounded flows? *Philosophical Transactions of the Royal Society A: Mathematical, Physical and Engineering Sciences*, 365(1852):789–806, 2007.
- [7] E. Hairer, S. Nørsett, and G. Wanner. *Solving ordinary differential equations: Nonstiff problems*, volume 1. Springer Verlag, 1993.
- [8] G. Heskestad. Hot-wire measurements in a plane turbulent jet. *Journal of Applied Mechanics*, 32:721, 1965.
- [9] J. Kim, P. Moin, and R. Moser. Turbulence statistics in fully developed channel flow at low reynolds number. *Journal of Fluid Mechanics*, 177(1):133–166, 1987.
- [10] A. Kolmogorov. The local structure of turbulence in incompressible viscous fluid for very large reynolds' numbers. In *Akademiia Nauk SSSR Doklady*, volume 30, pages 301–305, 1941.

- [11] E. Lanzinger and H. Langmack. Measuring air temperature by using an ultrasonic anemometer. *Poster presented at TECO-2005, Bucharest, Romania, available at: [http://www.umo.int/pages/prog/www/IMOP/publications/IOM-82-TECO\\\_2005/Posters/P](http://www.umo.int/pages/prog/www/IMOP/publications/IOM-82-TECO\_2005/Posters/P)*, 3.
- [12] X. Liu, F. Thomas, and R. Nelson. Measurement of the turbulence kinetic energy budget of symmetric planar wake flows in pressure gradient. In *APS Division of Fluid Dynamics Meeting Abstracts*, volume 1, 2000.
- [13] N. Mansour, J. Kim, and P. Moin. Reynolds-stress and dissipation-rate budgets in a turbulent channel flow. *Journal of Fluid Mechanics*, 194(1):15–44, 1988.
- [14] P. Mortensen. Particle dynamics in wall-bounded turbulence. Unpublished Doctoral Thesis, NTNU, 2007.
- [15] R. Moser and P. Moin. The effects of curvature in wall-bounded turbulent flows. *Journal of Fluid Mechanics*, 175(1):479–510, 1987.
- [16] S. Pope. *Turbulent flows*. Cambridge Univ Pr, 2000.
- [17] L. Richardson. *Weather prediction by numerical process*. Cambridge Univ Pr, 2007.
- [18] T. Shih, W. Liou, A. Shabbir, Z. Yang, and J. Zhu. A new k-[epsilon] eddy viscosity model for high reynolds number turbulent flows. *Computers & Fluids*, 24(3):227–238, 1995.
- [19] G. Taylor. Statistical theory of turbulence. *Proceedings of the Royal Society of London. Series A, Mathematical and Physical Sciences*, 151(873):421–444, 1935.
- [20] G. Taylor. The spectrum of turbulence. *Proceedings of the Royal Society of London. Series A-Mathematical and Physical Sciences*, 164(919):476–490, 1938.
- [21] H. Tennekes and J. Lumley. *A first course in turbulence*. The MIT press, 1972.
- [22] F. White. *Viscous fluid flow*, volume 3. McGraw-Hill New York, 2006.